Bulletin of the Seismological Society of America, Vol. 72, No. 6, pp. 2201–2226, December 1982

THE SANTA BARBARA, CALIFORNIA, EARTHQUAKE OF 13 AUGUST 1978

BY EDWARD J. CORBETT AND CARL E. JOHNSON

ABSTRACT

The 5.1 M_L Santa Barbara earthquake of 13 August 1978 occurred at 22^h54^m 52.8^s UTC. The epicenter was located 3 km southeast of Santa Barbara at 34° 23.9'N latitude and 119°40.9'W longitude with a focal depth of 12.7 km. The main shock was followed between 13 August and 30 September by 373 aftershocks that were located with the Caltech-USGS array. The aftershock zone extended 12 km WNW from the epicenter and was 6 km wide in the N-S direction, and it had a very clear temporal development. During the first 20 min of activity, all the aftershocks were located in a cluster 7 km WNW of the main shock epicenter. During the next 24 hr, the aftershock zone grew to 11 km in the WNW direction and 4 km in the N-S direction. During succeeding weeks, the zone extended to 12 by 6 km. This temporal-spatial development relative to the main shock epicenter may indicate that the initial rupture propagated 7 km unilaterally to the WNW, and the initial rupture plane may have been considerably smaller than the eventual aftershock zone. This smaller area suggests that the stress drop may have been significantly greater than that derived from the final aftershock zone.

In cross section, the aftershock hypocenters outline a nearly horizontal plane (dipping 15° or less) at 13 km depth. The main shock focal mechanism indicates NNE-SSW compression and vertical extension. The preferred fault plane strikes N80°W and dips 26°NNE, indicating north-over-south thrusting with a component of left-lateral movement. Focal mechanisms for 40 aftershocks also indicate compression in the general N-S direction. For most of these events, the north-dipping nodal plane dips between 7° and 45°, with most dipping 25° or more, which is significantly steeper than the plane delineated by the hypocenters themselves. These observations are consistent with a tectonic model in which much of the slip during the Santa Barbara earthquake occurred on a nearly horizontal plane. The after shocks then might represent movement on a complex series of imbricate thrust faults that flatten into the plane of primary slip. Hence, the Santa Barbara earthquake may be taken as evidence for mid-crustal horizontal shearing in the western Transverse Ranges.

INTRODUCTION

On the afternoon of 13 August 1978, the Santa Barbara area was shaken by a magnitude 5.1 M_L earthquake which caused moderate damage. The epicenter was located just offshore, 3 km southeast of Santa Barbara, with a hypocentral depth of nearly 13 km. The event was preceded by two foreshocks and was followed by over 300 aftershocks that were locatable using the Caltech-USGS seismographic network. This earthquake has been previously studied by Lee *et al.* (1978), but their locations for the main shock and aftershocks are systematically 4 km SW of our locations. This discrepancy is probably due to a strong contrast between the velocity structure in the Santa Barbara Channel and that on the mainland. We feel we have successfully corrected for that factor in this study.

Two fortunate circumstances allowed us to obtain high-quality locations for the main shock and many of its aftershocks. First, University of Southern California (USC) seismologists began deploying ocean bottom seismographs (OBS) in the

Santa Barbara Channel on the day before the earthquake, and four of them were in operation when the earthquake occurred (Henyey *et al.*, 1978). These stations were located almost directly above the activity and provided excellent data for controlling focal depths. Secondly, 1 month before the earthquake, a group from the University of California at Santa Barbara (UCSB) shot a seismic refraction line in the Santa Barbara Channel (Crandall *et al.*, 1979), and the arrival times at the onshore stations allowed us to calibrate the network for the velocity gradient in the Santa Barbara region. These two data sets greatly enhanced the location accuracy of the main shock and aftershocks, which enabled us to delineate the source mechanism involved in the Santa Barbara earthquake.

Geologic setting. The Santa Barbara earthquake occurred in the western end of

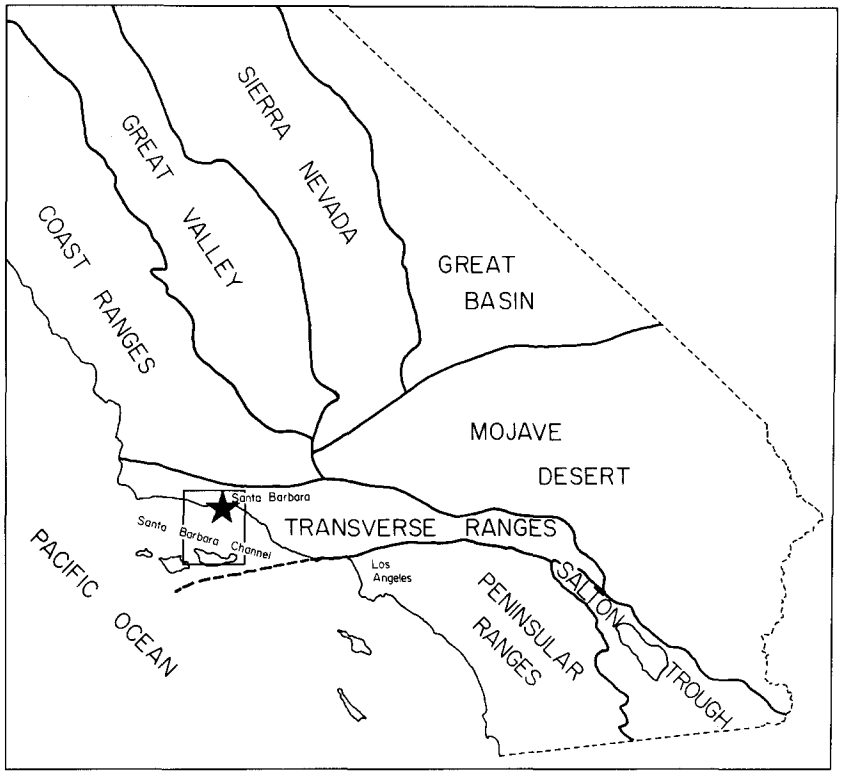

FIG. 1. Map showing geomorphic provinces of southern California and location of Santa Barbara earthquake (star). *Box* outlines area of this study.

the Transverse Ranges of southern California (Figure 1). This province is typified by geologically young mountain ranges and deep sedimentary basins that trend E-W, cutting across the NW-SE grain of most other geologic structures in California. The western Transverse Ranges include the Santa Ynez Mountains, located just north of Santa Barbara, the 700 m deep Santa Barbara Channel, and the Channel Islands. The geologic structure of the western Transverse Ranges is dominated by east-trending reverse faults, such as the Santa Ynez, Red Mountain, North Channel Slope-Pitas Point-Ventura, Mid-Channel, and Santa Cruz Island-Anacapa faults; all of these show signs of Quaternary activity (Jennings, 1975; Yerkes *et al.*, 1980). The recency of deformation is attested to by marine terraces, 45,000 to 2,500 yr in age, which indicate average uplift rates of 3 to 6 m per thousand years over this period

(Yerkes and Lee, 1979). Indeed, the Santa Barbara region is a tectonically active region, and hence the occurrence of the Santa Barbara earthquake is not surprising.

Previous seismicity. The Santa Barbara area is typified by abundant seismicity which has been previously studied by Hamilton *et al.* (1969), Sylvester *et al.* (1970), Lee and Vedder (1973), and Lee *et al.* (1979). The previous workers have shown that the seismicity is spatially diffuse and often occurs in swarms such as that in 1968 (Sylvester *et al.*, 1970). The seismic energy release apparently occurs by thrust movements on east-striking, north-dipping faults, which is in agreement with mapped geology in the region (Vedder *et al.*, 1969; Lee *et al.*, 1979). Of recent interest is a swarm that occurred in the Santa Barbara Channel beginning in late March 1978 and continued sporadically through July 1978 (Whitcomb *et al.*, 1979). The swarm was located 25 km SE of the August 1978 activity and was at the site of the small shock that preceded the 13 August main shock by 4 hr.

Velocity Model and Location Procedures

Previous velocity models. Previous seismicity studies (Lee and Vedder, 1973; Lee *et al.*, 1979) have used the regional crustal velocity model of Healy (1963). It consists of three layers over a half-space and was derived for a NW-SE line that passed along the California coast 50 km east of Santa Barbara. The preliminary study of this earthquake (Lee *et al.*, 1978) used a modification of this model that subdivided the upper two layers into seven layers to better approximate the velocity profile in the Santa Barbara Channel. Wallace *et al.* (1981) derived a velocity structure by inversion of the strong-motion records generated by the earthquake that was basically the same as that used by Lee *et al.* (1978). Most recently, Crandell *et al.* (1979) have determined the velocity structure of the eastern end of the Santa Barbara Channel from a seismic refraction profile. In contrast to all the above-mentioned models, they found that both the high-velocity lower crust and the Moho are 5 km shallower than has been previously observed. In addition, they observed a 7-km-thick cover of low-velocity sediments. Evidently, there is a dramatic change in the crustal structure between the onshore and offshore parts of the Santa Barbara region. This means that modeling the velocity structure as horizontal layers for the purpose of earthquake location computations will be, at best, difficult.

UCSB seismic refraction line. Since the explosions used in the Crandall *et al.* (1979) refraction study were detectable on the Caltech-USGS network, these were the best data to test the above-mentioned velocity models. On 16 July 1978, the *R. V. Ellen B. Scripps*, sailing from east to west along 34°18.5'N latitude, fired 10 shots (locations shown in Figure 2). Of these, nine could be reread from the Caltech archive magnetic tapes. The seismograms were retimed for 17 of the closest stations, which were 25 to 150 km from the shot points. The arrivals at the quiet stations were timed to an accuracy of 0.02 sec. The seismograms from the noisy stations (SBSC and SBSM in particular) were filtered with a 10-Hz low-pass filter which allowed the arrivals to be picked out from the noise more precisely. The filter was tested on seismograms from some of the quieter stations, and it was shown that arrival times were delayed, but by not more than 0.04 sec. Thus, it is believed that all arrivals, even those at the noisy stations, were picked to an accuracy of 0.10 sec. A few S arrivals were observed, but only rarely. Consequently only P-wave first arrivals were used in this study.

All four of the above-mentioned velocity models, as well as the Caltech Southern California model, were tested with this data set using the location program QED1 written by Johnson (1979). The explosions were first located using no station delays

and a depth of 0.5 km (average water depth along the traverse). In general, the results were poor, with the epicenters locating 1 to 5 km from the given explosion locations, usually biased toward the SW, with the mislocation problem getting worse toward the east end of the line (i.e., the area of interest). The results of using the Caltech Southern California model are indicated by the crosses in Figure 2. Of the five models, Healy's (1963) model located the explosions most accurately. It was, however, only marginally better, and gave large origin time errors (>+1 sec). Not surprisingly, the Crandall *et al.* (1979) model gave the best fit to origin times.

Next, an iterative process was used whereby station delays were determined from fixed locations. The locations and origin times of the shots were fixed to those given by UCSB, which reduced the number of useful events from nine to seven. The *P*

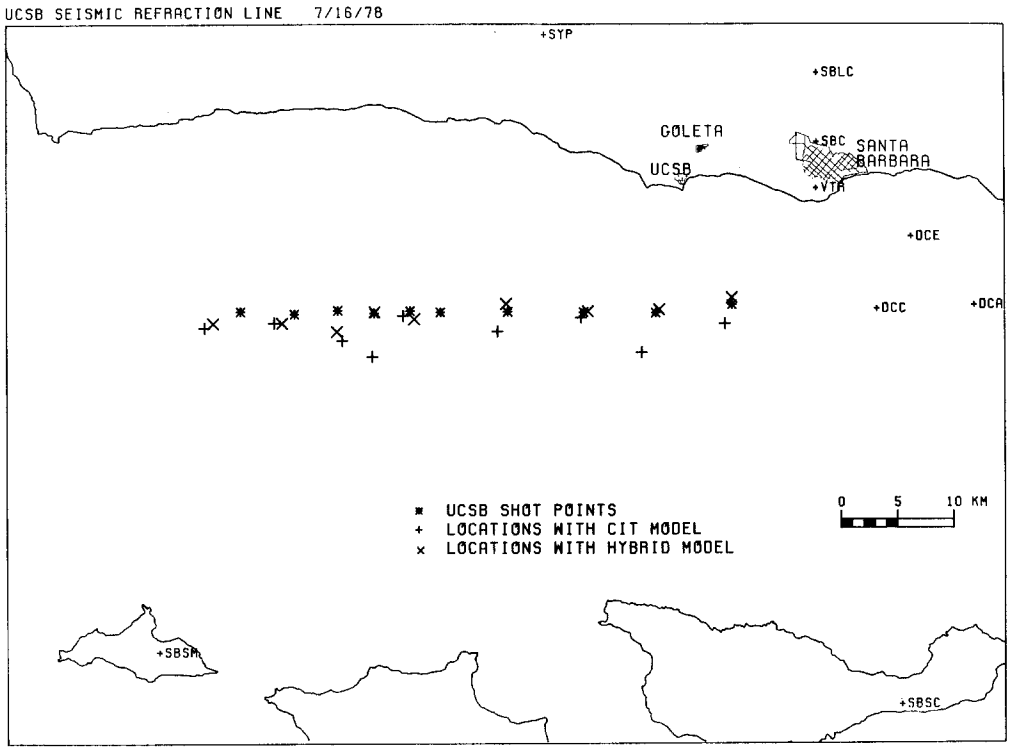

FIG. 2. Map comparing actual locations of shot points in UCSB seismic refraction line with calculated locations using Caltech's standard southern California velocity model and hybrid model of this study.

residuals for each station were considered, and the median value was taken as the *P* delay for that station. These station delays were then used in a freed solution to try and relocate the explosions. This method worked well for all velocity models, with most computed locations within 2 km of their true locations, and many within 0.5 km. Again, Healy's (1963) model relocated the explosions most accurately. However, this necessitated using large positive station delays (1 to 2 sec) for 11 of the 17 stations, indicating that this velocity profile does not adequately model the thick sedimentary pile in the eastern Santa Barbara Channel. On the other hand, the Crandall *et al.* (1979) structure appears to best model the travel times, since it requires small *P* delays (<0.15 sec) for 4 of the 5 stations around the perimeter of the channel. Unfortunately, this model does the poorest job of relocating the explosions, and indicates a systematic bias as one moves from east to west along the

refraction line. The relocations are shifted 1.5 km to the NE at the east end of the line, unshifted near the center, and shifted 3 km SW at the west end of the line. This effect may come from a systematic change in velocity structure along the axis of the channel, but it could also be caused by decreasing azimuthal control toward the west. Among other things, this exercise shows the difficulty of locating events within the Santa Barbara Channel using stations outside of the channel.

Hybrid velocity model. Although the Crandall *et al.* (1979) velocity structure is probably the one that is most appropriate within the Santa Barbara Channel, onshore there is a much thinner cover of low-density sediments. The higher velocity Moho and lower crust deepen rapidly, so Healy's (1963) model is probably more appropriate there. This is apparent in looking at the results of the above-mentioned attempt to fit the Crandall *et al.* (1979) model to the data. Stations beyond 70 km are required to have large positive residuals, indicating that the velocity model is too fast for the observed travel times. This discrepancy comes from the fact that the model would predict crossover to lower crust and Moho velocities for stations beyond 70 km, which is not observed. Since these more distant stations are reached by rays that travel deeper and travel more of their path in onshore crust than offshore crust, it was deemed appropriate to use a hybrid model that consists of Healy's (1963) model in the lower crust, and of the Crandall *et al.* (1979) model in the upper crust. This model is tabulated in Table 1.

TABLE 1

HYBRID VELOCITY MODEL

P-Wave Velocity (km/sec)	Depth of Top of Layer (km)
1.7	0.0
2.2	0.5
3.23	1.2
4.9	3.1
6.4	7.3
7.0	16.6
8.0	26.1

Determination of station delays. This model was used in the manner described above to determine *P* delays and to relocate the explosions. As shown in Figure 2, the four events at the east end of the line were located within 0.5 km of their given locations. The other five appear to get more and more biased to the south and west as one moves west. *P* delays obtained for this model are listed in the middle column of Table 2. Stations located on north and NE azimuths, such as ABL, BCH, and SBCC still have large positive delays, which indicates that velocities of this model are still not slow enough along these azimuths. Since the area of interest, however, is at the east end of the UCSB seismic refraction line, it is felt that this model locates the explosions to satisfactory accuracy.

This velocity model and set of station delays is a good starting model for locating the Santa Barbara earthquake sequence. It is, however, not completely appropriate because the *P* delays are derived for surface shots and not for an earthquake at depth. Consequently, it was necessary to use this starting model to pick a master event, which would in turn be used to locate the main shock and aftershocks in the manner described by Johnson and Hadley (1976).

Because the four USC stations (VTR, DCE, DCC, and DCA) had not yet been installed when the UCSB seismic line was run, we were not able to determine station delays for the OBSs. In trying to choose possible master events, it was

observed that the location solutions were unstable without the data from these four key stations, and it was not possible to evaluate which master events were better than the others. Consequently, we had to derive station delays for the four USC stations to use in the starting model. We did this by locating the main shock and first 12 hr of aftershocks using the hybrid model with delays, but without letting the OBSs constrain the solution. When an appropriate starting location was used, 47 events located reasonably well (ERZ < 2 km). The OBS station residuals for these best events were reviewed, and the median values were selected as the P delays. These are tabulated at the bottom of the second column in Table 2. Thus, we have a set of unconstrained P delays for the Caltech-USGS stations around the Santa

TABLE 2

STATION DELAYS RELATIVE TO HYBRID MODEL

Station Name	P-Delay (sec)	
	UCSB Seismic Refraction Line	Master Event 2311 13 August
ABL	0.71	—
BCH	1.05	1.00
BMT	—	1.30
CAM	0.32	0.41
CRG	—	1.77
ECF	0.43	0.35
FTC	—	0.39
KYP	−1.10	−0.82
PKM	0.42	0.41
PYR	0.25	0.63
RYS	0.58	0.44
SAD	—	−0.55
SBCC	0.78	0.92
SBCD	0.84	0.25
SBLC	−0.13	0.01
SBLG	−0.08	−0.92
SBLP	−0.14	−0.24
SBSC	−0.70	−1.11
SBSM	0.02	−1.14
SIP	−0.07	−0.01
SYP	−0.12	−0.21
YEG	—	1.52
VTR	−0.09*	−0.09
DCA	0.35*	0.34
DCC	0.12*	0.09
DCE	0.06*	0.08

* Delays derived from first 12 hr of aftershocks rather than UCSB seismic refraction line.

Barbara Channel and the USC stations in the channel to use as a starting model for locating the Santa Barbara activity.

Selection of master event. We located the main shock and aftershocks with this model and picked A- and B-quality events larger than magnitude 2.5 for consideration as possible master events. This step also gave us the averages, standard deviations, and medians of the P residuals for all of the stations. We then used this statistical information to evaluate each possible master event. From these, we selected six candidate master events: the main shock and five aftershocks, on the criterion that they gave consistent station residuals for the most stations, including

the 11 key stations in and around the channel. During this process, we observed that the residuals varied noticeably along the aftershock zone. In particular, as one moves from the main shock location to the NW, the residuals at SBSM and SBSC become more negative by 0.2 sec over a distance of only 6 km. This was observed for many of the possible master events and is, hence, believed to be systematic, further reflecting the velocity gradient in this area. This change is sufficient to appreciably affect the earthquake locations. Experimentation with the six candidate master events revealed that using the main shock as a master event would cause earthquake locations ~1 km SW of those that would result from selecting a master event that was located at the NW end of the aftershock zone. At this point, we picked the aftershock that occurred at 2311 UTC on 13 August as the master event because it was the one most centrally located within the aftershock zone. We used the residuals from this aftershock as station delays, according to the master event technique (Gardner, 1962; Johnson and Hadley, 1976), and located all 376 events using the location program QED1, the hybrid velocity model (Table 1), and the set of P delays indicated in the third column of Table 2. The calculated location parameters are listed in Table 3.

Earthquake Locations

Main shock. The Santa Barbara main shock occurred on 13 August 1978 at $22^h54^m52.8^s$ UTC. Our epicentral location is 34°23.9′N latitude and 119°40.9′W longitude (Figure 3) with a depth of 12.7 km. Due to the problems in modeling velocity, we conservatively estimate that the epicenter and depth may both be in error by as much as 2 km. Note that this location is 6 km NNE of that reported by Corbett and Johnson (1978) and 4.5 km NE of the location reported by Lee *et al.* (1978). It is in better agreement with Bogaert *et al.* (1978) and Henyey *et al.* (1978), who initially reported the epicenter to be closer to the Santa Barbara coastline.

Foreshocks. A search of Caltech-USGS network data for the 2 weeks prior to the main shock disclosed only two events that might be considered to be foreshocks. On 7 August at 1212 UTC, a magnitude 1.9 M_L event occurred under Santa Barbara. Its calculated location is 5 km NE of the main shock (Figure 3, *left*) with a depth of 12 km in a spot that is nearly absent of subsequent aftershocks. This event, however, was poorly recorded, and its location may be in error. The other event occurred at 1902 UTC on 13 August, 4 hr before the Santa Barbara earthquake. It was located 23 km SE of the main shock epicenter (Figure 3, *left*) at 8 km depth, and it had a magnitude of 2.4 M_L. Its location is of interest because it is a spot where there was considerable swarm activity in the preceding months, and we wonder if there was some causal relationship between the swarm activity, this foreshock, and the Santa Barbara earthquake. Most of the swarm activity occurred from 27 March to 15 April, but there was further sporadic activity in this same spot during late April, mid-June, and mid-July. The 13 August "foreshock" was the only event to occur here in all of August and September, and thus may have been the final shock of the swarm activity. In fact, the complete shutoff of activity in this area after 13 August may actually be more significant than the "foreshock" itself.

Aftershock locations. The data we studied allowed us to locate 376 events (Figure 3, *left*). These include 2 foreshocks, the main shock, and 373 aftershocks that occurred between 1 August and 30 September 1978. Of these locations, 159 were of quality A (Figure 3, *right*). We feel that the relative accuracy of the A-quality events is 0.5 km in both the horizontal and vertical directions, but due to possible errors in velocity modeling, the absolute inaccuracy may be as much as 2 km.

As can be seen in Figure 3, a couple of features disappear when we look at the

TABLE 3

SANTA BARBARA SEISMICITY (AUGUST–SEPTEMBER 1978)

YEAR	MO	DA	HR	MN	SEC	LATITUDE	LONGITUDE	DEPTH	MAG	GAP	NSTA	Q	RMS	ERH	ERZ	
1978	8	1	18	26	45.51	34 56.53	118 12.74	12.29		0	5	E	0.00	99.0	99.0	
1978	8	7	12	12	6.01	34 26.32	119 39.73	12.16	1.9	207	7	E	0.00	99.0	99.0	
1978	8	13	19	2	25.92	34 16.70	119 28.69	7.78	2.4	89	46	C	0.18	4.0	99.0	FORESHOCK?
1978	8	13	22	54	52.84	34 23.92	119 40.88	12.68	5.1	63	111	A	0.08	0.3	0.3	MAINSHOCK
1978	8	13	23	1	1.20	34 26.10	119 44.37	12.77	2.4	81	32	A	0.06	0.6	0.4	
1978	8	13	23	1	33.07	34 26.61	119 46.14	10.93		210	11	C	0.07	2.7	1.7	
1978	8	13	23	2	46.12	34 26.23	119 44.35	11.93	2.6	65	29	A	0.08	0.9	0.8	
1978	8	13	23	3	10.00	33 38.31	118 18.68	12.29		0	2	E	0.00	99.0	99.0	
1978	8	13	23	2	7.26	34 25.97	119 44.56	12.29		360	2	E	0.00	99.0	99.0	
1978	8	13	23	4	14.31	34 25.85	119 44.24	12.17		174	12	A	0.02	0.7	0.3	
1978	8	13	23	6	19.44	34 26.03	119 44.39	12.33	2.6	69	25	A	0.04	0.3	0.2	
1978	8	13	23	6	57.90	34 26.27	119 44.63	11.39	2.3	108	19	A	0.08	0.9	0.7	
1978	8	13	23	7	30.60	34 26.33	119 44.95	11.98	2.3	63	26	A	0.03	0.2	0.2	
1978	8	13	23	8	27.66	34 25.97	119 44.80	12.29	2.8	64	25	A	0.06	0.3	0.3	
1978	8	13	23	9	21.31	34 26.00	119 44.79	12.29	2.3	185	15	B	0.07	1.5	0.9	
1978	8	13	23	10	33.50	34 25.86	119 43.25	11.49	2.4	117	12	B	0.05	1.0	0.9	
1978	8	13	23	10	52.36	34 25.01	119 47.88	11.55		249	5	E	0.00	99.0	99.0	
1978	8	13	23	11	2.25	34 25.98	119 44.55	12.29	3.4	64	28	A	0.00	0.0	0.0	MASTER EVENT
1978	8	13	23	11	8.87	34 25.84	119 44.68	11.41	3.4	116	21	A	0.03	0.6	0.9	
1978	8	13	23	12	47.13	34 26.25	119 45.64	12.27		123	6	E	0.03	99.0	99.0	
1978	8	13	23	13	10.63	34 26.82	119 45.19	12.29		278	2	E	0.00	99.0	99.0	
1978	8	13	23	13	16.26	34 26.27	119 45.50	11.78		100	15	B	0.03	1.8	1.4	
1978	8	13	23	13	29.42	34 25.95	119 44.57	12.29		242	3	E	0.00	99.0	99.0	
1978	8	13	23	15	2.96	34 25.78	119 44.39	12.49	3.0	64	27	A	0.04	0.2	0.2	
1978	8	13	23	16	42.72	34 25.48	119 44.12	11.87	2.1	119	16	A	0.06	0.8	0.5	
1978	8	13	23	18	10.53	34 24.53	119 42.09	12.65	2.4	77	23	A	0.09	0.8	0.6	
1978	8	13	23	18	33.19	34 25.14	119 39.69	9.77	2.9	78	16	D	0.44	6.8	9.0	
1978	8	13	23	18	57.45	34 25.26	119 42.85	12.25	2.8	62	21	A	0.02	0.2	0.2	
1978	8	13	23	19	42.62	34 25.16	119 43.19	12.51	2.6	189	9	E	0.02	99.0	99.0	
1978	8	13	23	19	51.91	34 24.81	119 41.93	9.62		136	6	E	0.01	99.0	99.0	
1978	8	13	23	20	9.57	34 25.97	119 44.57	12.29		360	2	E	0.00	99.0	99.0	
1978	8	13	23	22	5.08	34 24.99	119 41.18	12.19		112	12	B	0.06	1.1	0.9	
1978	8	13	23	22	10.21	34 25.98	119 44.30	12.29	2.2	201	18	E	0.01	99.0	48.2	
1978	8	13	23	22	47.71	34 26.62	119 48.38	12.14	2.3	301	3	E	0.00	99.0	99.0	
1978	8	13	23	22	51.08	34 24.89	119 41.34	12.59	2.5	91	14	A	0.02	0.3	0.3	
1978	8	13	23	23	8.96	34 26.67	119 47.85	11.89	2.8	294	3	E	0.00	99.0	99.0	
1978	8	13	23	23	26.37	34 26.39	119 45.22	12.15	3.2	83	18	A	0.04	0.2	0.2	
1978	8	13	23	23	54.27	34 25.61	119 42.89	11.67	3.2	105	16	A	0.03	0.4	0.4	
1978	8	13	23	25	26.66	34 25.13	119 41.89	12.25	2.5	124	7	B	0.01	1.4	0.9	
1978	8	13	23	28	36.97	34 23.58	119 41.24	11.69	2.2	125	16	A	0.05	0.5	0.4	
1978	8	13	23	29	7.82	34 25.98	119 45.50	12.26		263	8	E	0.05	99.0	99.0	
1978	8	13	23	30	21.23	34 26.21	119 46.31	12.14	2.0	175	16	A	0.02	0.3	0.2	
1978	8	13	23	30	47.33	34 26.58	119 47.01	12.15	2.2	69	21	A	0.03	0.2	0.2	
1978	8	13	23	31	45.28	34 24.42	119 41.74	12.48	2.3	104	18	A	0.03	0.3	0.3	
1978	8	13	23	31	23.93	34 24.71	119 48.18	12.29		262	6	E	0.02	99.0	99.0	
1978	8	13	23	34	26.95	34 26.35	119 45.27	13.57	2.3	65	18	A	0.04	0.3	0.2	
1978	8	13	23	35	14.38	34 24.52	119 41.77	12.52		97	9	A	0.03	0.9	0.7	
1978	8	13	23	35	54.16	34 26.09	119 45.19	12.66	2.5	129	20	A	0.03	0.3	0.3	
1978	8	13	23	36	38.09	34 26.17	119 44.64	10.72	1.9	199	13	C	0.09	3.1	1.9	
1978	8	13	23	36	44.50	34 25.98	119 46.05	12.06	2.1	189	14	A	0.03	0.8	0.5	
1978	8	13	23	40	3.12	34 26.44	119 45.20	12.32	2.3	64	24	A	0.03	0.2	0.2	
1978	8	13	23	40	53.92	34 26.55	119 46.35	11.83		228	7	E	0.00	99.0	99.0	
1978	8	13	23	41	17.24	34 26.95	119 44.64	11.78		183	10	E	0.08	99.0	99.0	
1978	8	13	23	47	7.61	34 25.65	119 41.01	12.32	1.9	171	14	A	0.02	0.3	0.3	
1978	8	13	23	47	30.84	34 25.06	119 42.98	12.09		265	5	E	0.01	99.0	99.0	
1978	8	13	23	50	32.87	34 25.74	119 39.28	12.29	1.9	144	8	E	0.41	99.0	99.0	
1978	8	13	23	51	48.57	34 26.31	119 45.22	12.38	2.0	129	16	A	0.02	0.2	0.2	
1978	8	13	23	52	16.85	34 24.49	119 42.69	12.34	2.1	143	19	A	0.02	0.3	0.3	
1978	8	13	23	54	52.83	34 26.45	119 46.99	12.44	2.7	66	31	A	0.05	0.2	0.3	
1978	8	13	23	55	18.98	34 25.28	119 41.07	12.27	2.4	100	18	A	0.02	0.2	0.2	
1978	8	13	23	56	3.68	34 26.30	119 46.54	11.86	2.5	65	28	A	0.04	0.2	0.3	
1978	8	14	0	9	1.88	34 26.40	119 46.87	11.71	2.0	184	11	E	0.03	99.0	99.0	
1978	8	14	0	14	1.83	34 25.67	119 45.41	12.43	2.5	117	28	A	0.06	0.3	0.3	
1978	8	14	0	21	14.01	34 26.65	119 46.85	12.24	2.6	118	27	A	0.07	0.4	0.4	
1978	8	14	0	22	15.45	34 25.97	119 44.57	12.29		360	1	E	0.00	99.0	99.0	
1978	8	14	0	21	42.20	34 22.84	119 38.02	11.44		355	2	E	0.00	99.0	99.0	
1978	8	14	0	22	15.08	34 26.73	119 46.08	8.89		223	4	E	0.00	99.0	99.0	
1978	8	14	0	22	25.51	34 24.64	119 44.48	13.44	2.1	208	11	C	0.19	2.7	1.9	
1978	8	14	0	28	22.16	34 25.73	119 45.43	12.26	2.3	66	23	A	0.03	0.2	0.2	
1978	8	14	0	35	39.06	34 26.74	119 46.55	11.22	2.0	86	20	A	0.03	0.3	0.3	
1978	8	14	0	36	11.69	34 24.67	119 41.73	12.26		266	6	E	0.00	99.0	99.0	
1978	8	14	0	36	44.13	34 25.65	119 45.43	12.68	2.6	117	21	A	0.05	0.3	0.5	
1978	8	14	0	40	11.40	34 25.97	119 44.60	12.40	2.4	83	23	A	0.02	0.1	0.1	
1978	8	14	0	41	11.80	34 25.60	119 45.55	12.29		268	3	E	0.00	99.0	99.0	
1978	8	14	0	42	18.09	34 25.54	119 45.07	12.67	2.2	138	27	A	0.04	0.4	0.2	
1978	8	14	0	46	18.78	34 23.84	119 40.96	11.21	2.0	113	20	A	0.12	0.8	0.8	
1978	8	14	0	48	54.02	34 25.54	119 44.72	12.83	2.3	151	25	A	0.04	0.3	0.2	
1978	8	14	0	49	36.96	34 25.97	119 44.56	12.29		360	1	E	0.00	99.0	99.0	
1978	8	14	0	49	47.24	34 25.97	119 44.57	12.29		360	2	E	0.00	99.0	99.0	
1978	8	14	0	58	59.02	34 25.24	119 41.19	12.51	1.8	108	16	A	0.04	0.5	0.4	
1978	8	14	1	2	35.61	34 25.47	119 41.34	12.50	3.1	65	37	A	0.03	0.1	0.1	
1978	8	14	1	3	41.99	34 25.99	119 42.44	14.08	2.3	240	7	E	0.02	99.0	99.0	
1978	8	14	1	3	58.60	34 23.60	119 41.06	11.29	1.8	179	9	A	0.00	0.5	0.4	
1978	8	14	1	12	23.51	34 26.33	119 46.73	12.24	2.2	141	22	A	0.03	0.2	0.3	
1978	8	14	1	15	46.00	34 26.59	119 45.46	11.94	1.8	147	13	A	0.04	0.8	0.5	
1978	8	14	1	15	41.20	34 25.97	119 44.57	12.29		0	6	E	0.00	99.0	99.0	
1978	8	14	1	18	59.17	34 26.31	119 45.70	12.59	2.7	65	30	A	0.02	0.1	0.1	
1978	8	14	1	19	41.27	34 26.39	119 45.11	12.02	2.1	158	12	B	0.03	1.8	1.2	
1978	8	14	1	22	17.76	34 25.55	119 43.67	12.40	2.2	126	17	A	0.05	0.6	0.4	
1978	8	14	1	22	48.75	34 26.09	119 43.42	11.49		185	4	E	0.00	99.0	99.0	
1978	8	14	1	23	57.23	34 27.09	119 46.06	12.04	2.6	219	8	C	0.02	3.1	2.2	
1978	8	14	1	24	4.65	34 22.25	119 42.06	10.92	2.8	81	20	A	0.13	0.9	0.7	
1978	8	14	1	24	56.43	34 25.79	119 44.86	10.99		222	6	E	0.03	99.0	99.0	
1978	8	14	1	25	19.04	34 22.16	119 43.13	6.78		212	10	A	0.01	0.3	0.2	
1978	8	14	1	28	2.11	34 26.35	119 46.22	12.29	2.5	241	10	E	0.00	99.0	99.0	
1978	8	14	1	29	49.99	34 26.34	119 45.48	12.21	2.0	129	19	A	0.02	0.3	0.3	
1978	8	14	1	30	25.84	34 26.38	119 45.18	12.41	2.1	112	16	B	0.05	1.5	1.3	
1978	8	14	1	47	6.34	34 25.02	119 41.36	12.15	2.1	121	15	B	0.05	1.9	1.9	
1978	8	14	1	47	36.57	34 25.97	119 44.57	12.29		360	1	E	0.00	99.0	99.0	
1978	8	14	1	47	6.50	34 25.97	119 44.57	12.29		0	9	B	0.00	1.4	1.5	
1978	8	14	1	54	51.84	34 25.37	119 41.52	12.71	1.7	232	16	E	0.01	99.0	99.0	
1978	8	14	1	58	49.77	34 25.34	119 46.29	12.43	2.3	66	23	A	0.05	0.7	0.7	
1978	8	14	2	1	45.35	34 26.45	119 44.88	12.19	2.3	64	22	A	0.02	0.2	0.2	
1978	8	14	2	2	8.02	34 26.54	119 45.12	12.29	2.0	275	8	E	0.00	99.0	99.0	
1978	8	14	2	5	19.70	34 25.42	119 44.92	12.61	2.2	65	28	A	0.04	0.4	0.3	
1978	8	14	2	5	16.12	34 25.97	119 44.57	12.29	2.6	0	9	E	0.00	99.0	99.0	
1978	8	14	2	12	54.69	34 26.36	119 46.92	11.76	2.1	169	16	A	0.02	0.3	0.3	
1978	8	14	2	19	24.99	34 25.97	119 44.57	12.29		360	2	E	0.00	99.0	99.0	
1978	8	14	2	19	33.41	34 25.19	119 41.77	12.92	1.9	175	15	A	0.03	0.7	0.6	
1978	8	14	2	28	57.38	34 25.38	119 43.59	12.73	2.8	64	35	A	0.03	0.1	0.1	
1978	8	14	2	36	4.03	34 26.70	119 43.98	12.04	2.0	235	11	E	0.03	99.0	99.0	
1978	8	14	2	36	18.90	34 25.97	119 44.56	12.29		360	2	E	0.00	99.0	99.0	
1978	8	14	2	39	9.41	34 26.56	119 44.94	12.32	2.0	116	13	A	0.02	0.5	0.4	
1978	8	14	2	41	46.72	34 25.58	119 43.20	12.23	2.4	198	15	A	0.01	0.6	0.4	
1978	8	14	2	42	35.09	33 23.31	120 14.69	12.29		0	2	E	0.00	99.0	0.0	
1978	8	14	2	48	6.74	34 26.14	119 44.85	12.29	1.8	298	6	E	0.00	99.0	99.0	
1978	8	14	2	48	31.88	34 25.97	119 44.57	12.29		360	1	E	0.00	99.0	99.0	
1978	8	14	2	58	54.06	34 25.28	119 46.03	12.07	2.4	196	12	E	0.01	99.0	99.0	
1978	8	14	2	59	21.17	34 26.13	119 46.07	9.40	1.7	282	5	E	0.00	99.0	99.0	
1978	8	14	2	59	45.23	34 25.97	119 44.57	12.29		360	1	E	0.00	99.0	99.0	
1978	8	14	3	15	56.30	34 25.97	119 44.57	12.29		360	2	E	0.00	99.0	99.0	
1978	8	14	3	27	37.30	34 23.22	119 41.91	13.15	2.3	236	8	E	0.01	99.0	99.0	
1978	8	14	3	33	59.25	34 25.93	119 44.57	12.29	2.0	267	10	E	0.02	99.0	99.0	
1978	8	14	3	35	34.50	34 25.87	119 43.81	12.29	1.8	118	14	E	0.03	99.0	99.0	
1978	8	14	3	42	53.79	34 26.36	119 46.10	12.03	1.9	116	18	A	0.02	1.0	0.7	
1978	8	14	3	43	22.85	34 25.97	119 44.57	12.29		360	2	E	0.00	99.0	99.0	

YEAR	MO	DA	HR	MN	SEC	LATITUDE	LONGITUDE	DEPTH	MAG	GAP	NSTA	Q	RMS	ERH	ERZ
1978	8	14	3	43	28.13	34 25.97	119 44.56	12.29		360	1	E	0.00	99.0	99.0
1978	8	14	4	0	53.37	34 25.28	119 42.78	12.86	2.7	53	49	A	0.03	0.1	0.1
1978	8	14	4	9	11.86	34 26.11	119 44.97	12.55	1.7	238	13	E	0.03	99.0	99.0
1978	8	14	4	13	48.90	34 23.27	119 41.58	11.29	2.1	235	11	A	0.01	0.6	0.7
1978	8	14	4	14	6.09	34 26.22	119 47.34	12.06		346	3	E	0.00	99.0	99.0
1978	8	14	5	9	40.98	34 25.28	119 42.60	12.78	2.4	54	32	A	0.03	0.2	0.2
1978	8	14	5	22	42.51	34 25.09	119 41.89	12.38	2.8	61	36	A	0.04	0.2	0.2
1978	8	14	6	17	21.93	34 25.42	119 43.80	12.50	1.6	237	12	E	0.01	99.0	99.0
1978	8	14	6	33	27.23	34 25.79	119 42.55	12.29	2.4	57	29	A	0.04	0.2	0.2
1978	8	14	7	1	19.21	34 25.89	119 43.50	7.67	2.5	113	24	A	0.06	0.3	0.5
1978	8	14	7	3	15.84	34 25.59	119 43.46	12.52	2.5	63	28	A	0.04	0.2	0.2
1978	8	14	7	9	3.18	34 26.51	119 44.25	12.44	1.7	173	9	E	0.02	99.0	99.0
1978	8	14	7	45	51.14	34 26.26	119 46.32	12.29	2.5	65	24	A	0.03	0.2	0.2
1978	8	14	7	47	55.27	34 26.83	119 45.41	13.10	2.3	63	29	A	0.02	0.2	0.2
1978	8	14	7	54	53.30	34 26.14	119 45.93	12.29	2.3	67	30	A	0.03	0.2	0.3
1978	8	14	7	55	31.88	34 25.97	119 44.56	12.29		360	4	E	0.00	99.0	99.0
1978	8	14	8	31	20.90	34 26.09	119 45.49	11.58	2.0	183	15	A	0.03	0.4	0.3
1978	8	14	8	46	51.92	34 26.43	119 45.44	10.54	2.9	64	56	A	0.05	0.2	0.3
1978	8	14	9	32	28.43	34 25.23	119 42.71	12.33	2.3	63	27	A	0.03	0.2	0.2
1978	8	14	9	52	56.29	34 26.09	119 46.90	11.90	1.9	116	17	A	0.04	0.5	0.7
1978	8	14	10	14	6.10	34 26.54	119 46.84	11.96	1.9	116	14	A	0.04	0.4	0.5
1978	8	14	10	22	25.34	34 26.23	119 45.95	12.27		183	11	B	0.02	1.7	1.5
1978	8	14	10	22	29.59	34 25.99	119 47.85	13.95	2.0	189	20	A	0.03	0.9	0.9
1978	8	14	10	22	26.02	34 25.97	119 44.57	12.29		0	11	A	0.00	0.3	0.7
1978	8	14	10	25	13.12	34 25.71	119 44.16	12.48	2.3	64	31	A	0.06	0.5	0.6
1978	8	14	10	41	21.72	34 27.58	119 47.97	10.43	1.8	112	12	B	0.08	1.1	1.6
1978	8	14	10	54	1.75	34 26.41	119 46.22	11.84	1.9	131	20	A	0.02	0.2	0.2
1978	8	14	11	21	54.55	34 26.44	119 45.07	11.99	2.3	63	28	A	0.03	0.2	0.2
1978	8	14	12	24	34.55	34 17.43	119 42.78	11.73	1.7	140	17	C	0.19	3.4	3.6
1978	8	14	12	25	2.36	34 25.97	119 44.57	12.29		360	2	E	0.00	99.0	99.0
1978	8	14	12	43	10.63	34 26.36	119 45.28	12.18	1.9	116	18	A	0.02	0.2	0.2
1978	8	14	12	45	33.41	34 25.79	119 45.77	12.86	1.8	170	18	A	0.02	0.3	0.3
1978	8	14	12	53	42.66	34 25.60	119 44.21	12.34	2.7	64	42	A	0.06	0.3	0.3
1978	8	14	12	53	28.20	34 26.04	119 44.04	12.72	2.6	117	20	A	0.04	0.6	0.6
1978	8	14	13	20	31.71	34 26.51	119 43.35	13.20	2.0	116	14	A	0.04	0.6	0.6
1978	8	14	13	34	35.67	34 26.02	119 42.99	12.51	2.0	118	18	A	0.05	0.6	0.6
1978	8	14	13	58	5.30	34 26.45	119 45.39	12.24	1.9	123	11	A	0.02	0.5	0.5
1978	8	14	14	33	17.26	34 25.30	119 42.63	12.70	2.0	63	18	A	0.04	0.4	0.5
1978	8	14	15	10	11.72	34 27.21	119 38.23	11.96		341	2	E	0.00	99.0	99.0
1978	8	14	15	10	13.08	34 25.91	119 45.33	13.37	2.2	113	21	A	0.05	0.8	0.8
1978	8	14	15	10	53.30	34 25.97	119 44.56	12.29	1.9	360	2	E	0.00	99.0	99.0
1978	8	14	15	31	52.68	34 26.50	119 45.89	11.81	1.9	142	12	E	0.01	99.0	99.0
1978	8	14	15	37	21.50	34 26.37	119 44.76	12.67	2.1	180	15	E	0.01	99.0	99.0
1978	8	14	16	9	0.89	34 27.14	119 45.86	11.94		239	5	E	0.00	99.0	99.0
1978	8	14	16	9	47.10	33 20.79	119 48.91	12.29		0	3	E	0.00	99.0	0.0
1978	8	14	16	9	52.71	34 27.21	119 45.47	12.29		285	2	E	0.00	99.0	99.0
1978	8	14	16	11	38.51	34 25.97	119 44.57	12.29		360	1	E	0.00	99.0	99.0
1978	8	14	16	55	1.24	34 20.94	119 48.84	13.22	2.5	78	25	A	0.10	0.6	1.0
1978	8	14	17	3	58.95	34 26.34	119 43.48	14.66	2.2	118	7	E	0.03	99.0	99.0
1978	8	14	17	4	10.61	34 26.51	119 44.86	12.23	2.3	116	21	A	0.02	0.4	0.2
1978	8	14	17	21	31.99	34 26.75	119 43.68	9.63	2.3	116	16	A	0.03	0.5	0.5
1978	8	14	17	26	57.59	34 22.07	119 49.02	10.45	2.4	120	23	B	0.15	1.6	2.8
1978	8	14	17	27	35.08	34 25.78	119 43.83	12.56	2.2	64	18	A	0.06	0.8	0.8
1978	8	14	18	35	39.57	34 26.28	119 45.83	12.06	1.7	183	13	A	0.01	0.6	0.5
1978	8	14	19	0	3.00	34 26.34	119 46.32	11.99	2.1	65	23	A	0.02	0.3	0.3
1978	8	14	19	0	44.87	34 25.97	119 44.56	12.29		360	2	E	0.00	99.0	99.0
1978	8	14	19	34	53.71	34 25.77	119 43.41	12.30	1.6	180	9	E	0.02	99.0	99.0
1978	8	14	19	35	27.30	34 25.97	119 44.56	12.29		360	1	E	0.00	99.0	99.0
1978	8	14	19	34	53.06	34 25.97	119 44.57	12.29		0	2	E	0.00	99.0	99.0
1978	8	14	19	50	54.39	34 25.97	119 44.57	12.29		360	2	E	0.00	99.0	99.0
1978	8	14	20	22	52.77	34 25.97	119 43.25	12.39	1.9	118	14	B	0.03	1.2	0.8
1978	8	14	20	25	44.94	34 26.08	119 45.75	12.29		335	3	E	0.00	99.0	99.0
1978	8	14	20	25	53.85	34 25.97	119 44.57	12.29		360	2	E	0.00	99.0	99.0
1978	8	14	20	26	5.50	34 25.97	119 44.57	12.29		360	2	E	0.00	99.0	99.0
1978	8	14	21	5	31.73	34 25.37	119 43.86	12.33	1.7	178	12	E	0.02	99.0	99.0
1978	8	14	21	5	56.55	34 20.03	119 48.96	12.24		219	7	E	0.18	99.0	99.0
1978	8	14	21	13	10.83	34 26.44	119 47.03	11.65	1.7	184	11	E	0.01	99.0	99.0
1978	8	14	21	13	32.94	34 25.97	119 44.56	12.29		360	2	E	0.00	99.0	99.0
1978	8	14	23	58	33.58	34 26.42	119 45.11	12.29		324	5	E	0.00	99.0	99.0
1978	8	15	0	22	59.36	34 25.97	119 44.56	12.29		360	1	E	0.00	99.0	9.4
1978	8	15	0	32	39.96	34 25.97	119 44.57	12.29		360	2	E	0.00	99.0	99.0
1978	8	15	1	18	36.01	34 27.38	119 47.18	12.55	2.1	242	12	B	0.02	1.6	0.7
1978	8	15	1	19	34.04	34 26.29	119 44.76	12.31	2.1	265	5	E	0.01	99.0	99.0
1978	8	15	2	28	18.47	34 25.41	119 42.64	12.12	2.1	114	14	A	0.03	0.6	0.5
1978	8	15	4	26	9.24	34 21.45	119 48.50	7.50	1.8	155	12	E	0.06	99.0	99.0
1978	8	15	4	37	13.77	34 22.12	119 49.44	8.26	2.3	120	17	D	0.19	9.8	99.0
1978	8	15	4	37	48.96	34 21.54	119 47.37	10.92	2.2	127	11	E	0.10	99.0	99.0
1978	8	15	5	40	17.05	34 25.60	119 41.05	12.54	2.2	106	16	A	0.02	0.6	0.5
1978	8	15	6	25	57.86	34 21.65	119 48.67	12.88	2.4	122	22	A	0.10	0.8	1.0
1978	8	15	7	0	52.50	34 25.97	119 44.57	12.29		360	2	E	0.00	99.0	9.4
1978	8	15	8	14	11.65	34 26.17	119 44.06	12.70	1.7	119	15	B	0.04	1.9	1.5
1978	8	15	9	58	32.54	34 26.09	119 45.48	12.56	2.4	64	36	A	0.03	0.2	0.2
1978	8	15	12	9	25.56	34 25.77	119 43.95	12.29	2.1	114	15	E	0.03	99.0	99.0
1978	8	15	13	7	56.57	34 25.97	119 44.56	12.29		360	2	E	0.00	99.0	99.0
1978	8	15	15	52	46.23	34 26.16	119 44.99	12.42	2.2	64	18	A	0.02	0.1	0.1
1978	8	15	17	16	43.35	34 25.28	119 42.80	12.44	2.2	90	21	A	0.02	0.2	0.2
1978	8	15	18	48	31.34	34 25.68	119 44.48	12.29		316	7	E	0.06	99.0	99.0
1978	8	15	19	1	42.96	34 21.54	119 48.52	12.35	2.2	155	8	E	0.01	99.0	99.0
1978	8	15	19	1	40.66	34 25.97	119 44.57	12.29		0	8	E	0.00	99.0	99.0
1978	8	16	0	39	34.23	34 25.53	119 43.81	12.33	2.2	81	20	A	0.06	0.6	0.5
1978	8	16	1	47	4.02	34 26.09	119 43.53	12.36	1.7	118	9	E	0.02	99.0	99.0
1978	8	16	1	57	12.77	34 25.87	119 43.46	12.59	2.0	235	9	E	0.02	99.0	99.0
1978	8	16	4	24	29.85	34 23.49	119 41.47	12.17	2.2	127	22	A	0.06	0.8	1.1
1978	8	16	5	31	6.88	34 17.14	119 41.96	12.29	2.5	77	26	B	0.17	1.0	1.1
1978	8	16	7	43	35.34	34 26.33	119 44.98	12.37	2.0	116	15	A	0.02	0.3	0.3
1978	8	16	8	10	54.15	34 21.64	119 47.63	8.47	2.0	146	12	E	0.07	99.0	99.0
1978	8	16	8	57	57.63	34 21.04	119 47.90	8.77	2.2	149	15	D	0.05	7.1	99.0
1978	8	16	9	57	28.85	34 23.24	119 41.44	11.29	2.2	65	25	A	0.09	0.6	0.6
1978	8	16	10	43	37.90	34 25.89	119 43.63	12.66	1.9	113	20	B	0.06	1.2	1.1
1978	8	16	10	55	17.20	34 26.61	119 44.13	13.55	1.9	117	18	A	0.02	0.6	0.4
1978	8	16	11	40	28.44	34 25.51	119 43.85	12.43	2.7	64	52	A	0.04	0.3	0.2
1978	8	16	12	45	13.97	34 22.99	119 42.21	12.11		237	7	E	0.02	99.0	99.0
1978	8	16	13	35	12.09	34 26.35	119 46.30	12.51	3.3	65	44	A	0.04	0.2	0.2
1978	8	16	13	36	10.80	34 27.57	119 45.72	12.29	2.5	291	4	E	0.00	99.0	99.0
1978	8	16	15	36	58.50	34 26.39	119 44.30	12.29	2.3	130	8	E	0.02	99.0	99.0
1978	8	16	19	12	39.85	34 26.08	119 43.84	12.29	1.7	220	5	E	0.00	99.0	99.0
1978	8	16	21	45	13.87	34 25.97	119 44.56	12.29		360	2	E	0.00	99.0	9.4
1978	8	17	2	0	9.47	34 26.90	119 42.25	10.92	2.2	259	10	E	0.01	99.0	99.0
1978	8	17	2	58	6.42	34 26.19	119 47.41	13.38	2.6	66	31	A	0.06	0.3	0.3
1978	8	17	4	48	25.94	34 25.54	119 43.37	12.29	1.8	235	18	A	0.01	0.5	0.3
1978	8	17	8	44	4.01	34 25.97	119 44.57	12.29		360	2	E	0.00	99.0	99.0
1978	8	17	8	53	37.33	34 23.34	119 41.81	11.65	2.0	129	19	A	0.04	0.9	1.0
1978	8	17	11	40	5.87	34 26.15	119 44.37	9.73	1.7	180	11	A	0.01	0.5	0.5
1978	8	17	12	52	8.65	34 25.47	119 44.28	12.42	2.4	128	28	A	0.02	0.1	0.1
1978	8	17	15	57	42.96	34 26.78	119 45.93	12.29		312	4	E	0.00	99.0	99.0
1978	8	17	18	2	46.66	34 26.05	119 44.67	11.94	2.1	86	16	E	0.04	99.0	99.0
1978	8	17	18	30	27.00	34 25.96	119 44.92	11.80	2.0	129	11	E	0.01	99.0	99.0
1978	8	17	19	32	3.99	34 25.13	119 42.43	11.93	2.2	181	7	E	0.00	99.0	99.0
1978	8	17	21	40	6.36	34 26.74	119 44.55	12.29		216	3	E	0.00	99.0	99.0
1978	8	17	21	52	59.51	34 25.08	119 44.58	12.03	2.0	185	16	E	0.01	99.0	99.0
1978	8	17	21	53	35.07	34 25.97	119 44.56	12.29		360	1	E	0.00	99.0	99.0
1978	8	17	23	28	15.36	34 24.66	119 41.40	11.74	2.2	122	18	A	0.03	0.6	0.7
1978	8	18	0	31	13.48	34 26.31	119 44.58	12.02	1.8	237	11	E	0.01	99.0	99.0
1978	8	18	1	55	6.49	34 26.38	119 45.99	12.51	2.2	67	20	A	0.03	0.2	0.2
1978	8	18	2	24	22.30	34 26.67	119 44.58	12.83	2.2	79	15	A	0.05	0.6	0.6
1978	8	18	2	24	40.79	34 25.97	119 44.57	12.29	2.0	360	8	E	0.00	99.0	99.0

TABLE 3—*Continued*

YEAR	MO	DA	HR	MN	SEC	LATITUDE	LONGITUDE	DEPTH	MAG	GAP	NSTA	Q	RMS	ERH	ERZ
1978	8	18	2	52	50.72	34 26.03	119 43.67	12.47	1.8	124	10	B	0.02	1.1	0.8
1978	8	18	7	18	51.79	34 25.88	119 44.00	12.58	2.2	81	28	A	0.03	0.2	0.2
1978	8	18	8	16	34.57	34 26.24	119 43.71	12.45	1.8	124	18	B	0.05	1.0	0.8
1978	8	18	8	53	46.02	34 26.15	119 45.67	12.18	1.8	178	16	B	0.02	1.0	0.8
1978	8	18	11	17	5.99	34 26.01	119 43.76	12.26	1.7	118	15	C	0.09	3.0	2.7
1978	8	18	11	54	51.03	34 26.29	119 46.09	12.06	2.1	117	16	A	0.02	0.3	0.3
1978	8	18	13	20	59.67	34 26.15	119 44.51	12.75	1.9	149	10	E	0.01	99.0	99.0
1978	8	18	16	12	49.52	34 26.22	119 47.36	12.01	2.3	66	19	A	0.03	0.3	0.4
1978	8	18	18	40	1.62	34 25.90	119 43.63	12.16	2.3	113	16	A	0.02	0.8	0.6
1978	8	18	22	17	58.84	34 25.60	119 44.21	12.34	1.9	183	11	B	0.03	2.0	1.5
1978	8	18	23	37	7.72	34 25.99	119 45.08	12.53	1.9	183	16	B	0.06	1.8	1.1
1978	8	18	23	37	1.10	34 25.97	119 44.57	12.29	1.7	0	6	E	0.00	99.0	99.0
1978	8	18	23	37	41.82	34 25.97	119 44.57	12.29		360	1	E	0.00	99.0	99.0
1978	8	19	0	0	30.10	34 26.51	119 45.63	12.12	2.2	116	15	E	0.04	99.0	99.0
1978	8	19	1	52	31.43	34 27.19	119 46.12	12.78	1.8	178	10	E	0.01	99.0	99.0
1978	8	19	14	59	42.60	34 25.97	119 44.57	12.29		360	2	E	0.00	99.0	99.0
1978	8	19	14	59	40.98	35 49.86	119 17.57	12.29	2.3	360	17	E	0.00	99.0	99.0
1978	8	19	16	17	35.86	34 25.22	119 42.71	12.22	2.0	113	16	A	0.02	0.3	0.3
1978	8	19	22	22	28.54	34 26.00	119 44.84	12.36	1.8	185	10	E	0.02	99.0	99.0
1978	8	19	22	49	0.84	34 25.84	119 43.06	12.22	1.7	235	12	E	0.01	99.0	99.0
1978	8	19	22	56	22.85	34 25.61	119 43.85	12.87	1.8	237	12	E	0.01	99.0	99.0
1978	8	20	2	9	58.34	34 26.27	119 46.60	12.06	2.3	116	25	A	0.02	0.4	0.4
1978	8	20	4	4	52.87	34 25.73	119 43.72	12.69	2.1	181	15	A	0.02	0.9	0.6
1978	8	20	13	14	55.54	34 25.16	119 42.76	12.12	2.2	63	25	A	0.03	0.3	0.3
1978	8	20	16	20	58.59	34 25.50	119 46.56	11.98	1.9	118	18	B	0.04	1.3	1.6
1978	8	20	20	15	46.47	34 25.68	119 44.43	12.57	3.1	65	37	A	0.04	0.2	0.2
1978	8	20	23	21	53.30	34 25.81	119 44.31	12.35	1.8	182	16	B	0.01	1.1	0.8
1978	8	21	0	4	52.37	34 24.79	119 43.07	12.68	1.9	128	14	E	0.02	99.0	99.0
1978	8	21	0	6	37.84	34 25.20	119 42.81	12.49	1.8	185	10	E	0.02	99.0	99.0
1978	8	21	7	34	7.30	34 26.11	119 47.22	11.93	1.9	186	13	E	0.01	99.0	99.0
1978	8	21	7	41	19.28	34 26.21	119 47.32	12.23	2.6	66	35	A	0.04	0.3	0.4
1978	8	21	8	10	7.53	34 26.34	119 46.38	12.01	1.8	184	15	E	0.01	99.0	99.0
1978	8	21	13	32	36.57	34 25.42	119 42.00	12.99	1.9	115	18	A	0.04	0.6	0.6
1978	8	21	17	17	57.51	34 25.88	119 43.61	12.50	1.8	118	13	E	0.01	99.0	99.0
1978	8	21	18	56	29.86	34 21.30	119 48.15	8.86	2.1	155	14	E	0.03	99.0	99.0
1978	8	21	19	23	5.29	34 21.42	119 48.83	13.77	2.0	127	6	E	0.01	99.0	99.0
1978	8	21	19	37	18.17	34 20.94	119 34.55	13.64		265	5	E	0.00	99.0	99.0
1978	8	21	22	54	2.73	34 21.56	119 48.40	9.83	2.1	155	11	E	0.05	99.0	99.0
1978	8	22	3	28	12.98	34 27.47	119 46.38	12.84	1.7	177	14	E	0.02	99.0	99.0
1978	8	22	5	16	18.91	34 25.01	119 43.22	12.67	1.5	236	10	E	0.00	99.0	99.0
1978	8	22	17	32	23.11	34 25.41	119 48.49	11.74	2.1	255	12	E	0.02	99.0	99.0
1978	8	22	22	17	2.84	34 25.97	119 44.56	12.29		360	2	E	0.00	99.0	99.0
1978	8	23	4	25	10.00	34 26.67	119 44.02	7.26	2.0	176	13	B	0.03	1.4	0.7
1978	8	23	9	59	1.22	34 25.87	119 44.50	12.58	2.3	64	25	A	0.03	0.4	0.4
1978	8	23	13	25	32.19	34 26.18	119 45.88	12.08	2.4	65	18	A	0.03	0.3	0.4
1978	8	23	13	26	9.44	34 26.07	119 45.79	11.90	2.1	65	15	A	0.03	0.5	0.5
1978	8	23	14	29	17.46	34 25.97	119 44.57	12.29		360	1	E	0.00	99.0	99.0
1978	8	23	14	29	37.19	34 25.88	119 45.21	12.29		270	3	E	0.00	99.0	99.0
1978	8	23	16	17	11.65	34 28.13	119 44.14	13.18	1.9	139	9	E	0.01	99.0	99.0
1978	8	23	23	44	6.42	34 27.10	119 41.40	12.29	1.9	230	10	E	0.00	99.0	99.0
1978	8	24	0	17	13.14	34 27.74	119 46.75	12.49	2.3	64	22	A	0.05	0.5	0.5
1978	8	24	2	29	51.84	34 25.97	119 44.57	12.29		360	1	E	0.00	99.0	99.0
1978	8	24	2	36	56.67	34 26.17	119 45.59	12.40	2.4	66	23	A	0.02	0.2	0.2
1978	8	24	13	37	31.42	34 26.81	119 44.55	13.33	2.1	116	13	B	0.04	1.1	0.9
1978	8	25	5	37	7.22	34 26.06	119 47.35	11.94	2.0	187	7	E	0.01	99.0	99.0
1978	8	25	9	27	57.95	34 25.36	119 44.18	12.36	1.9	183	11	E	0.02	99.0	99.0
1978	8	25	12	20	43.61	34 28.79	119 52.85	11.73	2.1	130	11	E	0.06	99.0	99.0
1978	8	25	17	43	27.23	34 26.83	119 45.93	13.93	2.0	124	8	E	0.01	99.0	99.0
1978	8	26	3	40	53.03	34 26.12	119 44.15	12.71	1.8	262	13	E	0.02	99.0	99.0
1978	8	26	16	26	38.42	34 26.86	119 46.37	13.09	2.7	64	27	A	0.05	0.4	0.4
1978	8	26	23	38	49.16	34 21.79	119 43.46	6.94	1.7	251	14	E	0.06	99.0	99.0
1978	8	28	0	44	37.06	34 22.46	119 40.83	13.01	2.1	235	11	E	0.03	99.0	99.0
1978	8	28	2	47	53.60	34 27.64	119 45.90	12.42	1.7	238	7	E	0.01	99.0	99.0
1978	8	28	8	39	49.36	34 22.81	119 42.14	11.64	1.9	237	11	E	0.02	99.0	99.0
1978	8	28	9	33	1.38	34 25.76	119 43.41	12.45	2.3	113	24	A	0.03	0.3	0.3
1978	8	28	22	58	21.82	34 26.92	119 47.01	12.72	1.9	190	8	E	0.02	99.0	99.0
1978	8	29	3	18	53.65	34 25.32	119 42.56	12.38	2.1	175	18	A	0.04	0.5	0.5
1978	8	29	3	57	49.81	34 27.32	119 46.31	12.50	1.7	178	9	E	0.02	99.0	99.0
1978	8	29	5	47	9.77	34 25.47	119 44.42	12.51	2.0	179	13	B	0.03	1.8	1.6
1978	8	29	6	4	49.06	34 26.34	119 44.70	13.89	2.8	64	34	A	0.04	0.3	0.3
1978	8	29	8	46	39.58	34 26.27	119 43.71	7.39	2.1	117	15	D	0.06	9.4	99.0
1978	8	29	10	51	45.33	34 26.98	119 47.11	13.66	2.6	114	22	A	0.03	0.3	0.3
1978	8	29	15	28	57.05	34 26.94	119 45.65	13.00	2.0	239	7	E	0.02	99.0	99.0
1978	8	29	17	20	54.12	34 26.88	119 40.98	12.36	1.9	171	12	E	0.03	99.0	99.0
1978	8	29	19	3	58.44	34 25.79	119 44.41	12.29	2.2	118	10	E	0.03	99.0	99.0
1978	8	29	23	6	58.37	34 26.45	119 44.69	12.29	2.3	63	28	A	0.05	0.6	0.6
1978	8	30	1	23	5.54	34 26.19	119 44.83	12.26	1.9	126	12	A	0.02	0.7	0.5
1978	8	30	10	54	36.11	34 28.26	119 46.13	12.72	2.0	126	11	E	0.02	99.0	99.0
1978	8	31	13	11	23.78	34 25.48	119 43.51	10.36	2.1	237	13	E	0.15	99.0	99.0
1978	8	31	16	37	6.49	34 13.28	119 43.74	20.17	2.5	90	32	A	0.08	0.5	0.8
1978	8	31	22	0	5.31	34 25.97	119 44.57	12.29		360	2	E	0.00	99.0	99.0
1978	9	1	8	15	59.85	34 26.82	119 46.49	12.18	2.0	176	7	E	0.00	99.0	99.0
1978	9	1	13	17	14.14	34 21.38	119 24.16	10.86	2.0	208	11	E	0.05	99.0	99.0
1978	9	1	22	32	35.66	34 27.08	119 46.47	13.45	2.1	114	10	E	0.03	99.0	99.0
1978	9	1	22	57	55.32	34 26.62	119 44.11	13.63		119	7	E	0.04	99.0	99.0
1978	9	2	7	6	25.40	34 27.37	119 46.75	12.49	1.9	120	18	E	0.06	99.0	99.0
1978	9	3	10	11	17.50	34 23.11	119 41.81	9.42	2.1	145	13	A	0.02	0.3	0.9
1978	9	3	15	25	4.92	34 26.22	119 44.43	12.29	2.0	144	7	E	0.02	99.0	99.0
1978	9	3	18	37	10.31	34 26.45	119 43.94	12.56	2.0	119	12	E	0.01	99.0	99.0
1978	9	4	3	26	7.05	34 26.50	119 46.45	13.23	2.1	169	15	A	0.01	0.4	0.3
1978	9	5	5	38	7.51	34 25.73	119 42.93	12.13	2.2	168	18	A	0.03	0.6	0.5
1978	9	5	8	6	17.77	34 12.93	119 42.60	19.49	2.8	88	31	A	0.11	0.7	1.1
1978	9	5	14	35	24.23	34 25.81	119 44.52	12.29	2.1	118	12	E	0.04	99.0	99.0
1978	9	5	20	19	50.43	34 25.65	119 43.73	11.59	2.3	80	23	A	0.06	0.5	0.5
1978	9	6	18	57	40.46	34 27.02	119 47.24	10.90	2.2	127	13	A	0.05	0.8	1.1
1978	9	7	1	0	11.67	34 25.57	119 41.08	12.29	2.3	58	26	A	0.04	0.3	0.3
1978	9	7	12	32	30.17	34 23.35	119 57.46	15.13		149	8	E	0.22	99.0	99.0
1978	9	7	19	0	20.02	34 26.16	119 43.73	13.20	2.5	124	36	A	0.04	0.2	0.2
1978	9	7	23	23	2.60	34 25.47	119 41.72	13.56	2.0	233	9	E	0.03	99.0	99.0
1978	9	8	23	35	23.80	34 25.56	119 41.33	12.70	1.9	177	8	E	0.04	99.0	99.0
1978	9	10	15	28	41.16	34 28.37	119 46.48	11.84	2.5	79	23	A	0.05	0.5	0.4
1978	9	11	4	19	38.19	34 27.74	119 45.83	11.76	2.2	131	24	A	0.06	0.4	0.4
1978	9	11	11	51	30.01	34 27.79	119 44.88	12.10	2.0	285	9	E	0.02	99.0	99.0
1978	9	11	18	27	38.82	34 25.08	119 46.49	11.13	1.9	190	9	E	0.00	99.0	99.0
1978	9	12	11	57	54.74	34 28.11	119 45.02	14.28	3.4	112	74	A	0.09	0.5	0.4
1978	9	14	1	7	4.61	34 11.12	119 37.09	15.33	2.2	162	11	A	0.04	0.7	0.7
1978	9	15	11	39	27.54	34 25.97	119 44.56	12.29		360	2	E	0.00	99.0	28.7
1978	9	15	14	33	39.48	34 26.31	119 43.62	13.26	2.0	78	14	A	0.03	0.8	0.6
1978	9	16	1	31	51.39	34 26.50	119 46.19	14.56	2.0	286	12	E	0.00	99.0	99.0
1978	9	16	9	19	49.84	34 25.92	119 46.78	11.75	1.8	186	12	E	0.01	99.0	99.0
1978	9	16	9	48	2.77	34 22.44	119 42.05	10.50	2.8	116	33	A	0.09	0.5	0.6
1978	9	16	9	49	15.68	34 24.09	119 42.86	12.69	1.8	276	8	E	0.00	99.0	99.0
1978	9	16	13	59	50.02	34 25.97	119 44.57	12.29	2.6	0	29	D	0.00	26.9	26.9
1978	9	16	13	59	45.05	34 27.24	119 44.61	12.28		304	6	E	0.02	99.0	99.0
1978	9	17	15	7	53.79	34 25.97	119 44.57	12.29		360	1	E	0.00	99.0	99.0
1978	9	18	1	38	30.19	34 26.27	119 45.32	12.50	2.4	65	28	A	0.08	0.8	0.6
1978	9	20	4	18	44.95	34 25.08	119 41.39	12.06	2.3	61	27	A	0.06	0.5	0.4
1978	9	22	3	5	3.18	34 29.89	119 44.57	12.29	2.2	307	5	E	0.03	99.0	99.0
1978	9	22	14	57	18.53	34 26.46	119 43.16	13.35	1.8	249	6	E	0.00	99.0	99.0
1978	9	23	17	40	40.50	34 26.36	119 40.76	5.31	2.0	204	12	E	0.04	99.0	99.0
1978	9	24	2	4	26.90	34 26.63	119 44.07	10.26	3.5	113	78	A	0.06	0.3	0.4
1978	9	26	0	2	38.47	34 26.83	119 45.50	12.34	1.9	179	10	E	0.00	99.0	99.0
1978	9	26	14	36	14.53	34 25.86	119 44.36	12.29	1.9	252	3	E	0.00	99.0	99.0
1978	9	28	15	36	1.92	34 26.27	119 43.68	13.16	2.0	178	16	B	0.04	1.4	1.0
1978	9	28	21	23	52.59	34 26.21	119 45.94	12.11	1.8	183	13	E	0.00	99.0	99.0
1978	9	29	11	6	25.42	34 26.55	119 47.78	12.13	2.0	120	19	A	0.02	0.4	0.4
1978	9	30	1	35	10.11	34 26.14	119 45.50	12.31	1.8	183	12	E	0.01	99.0	99.0

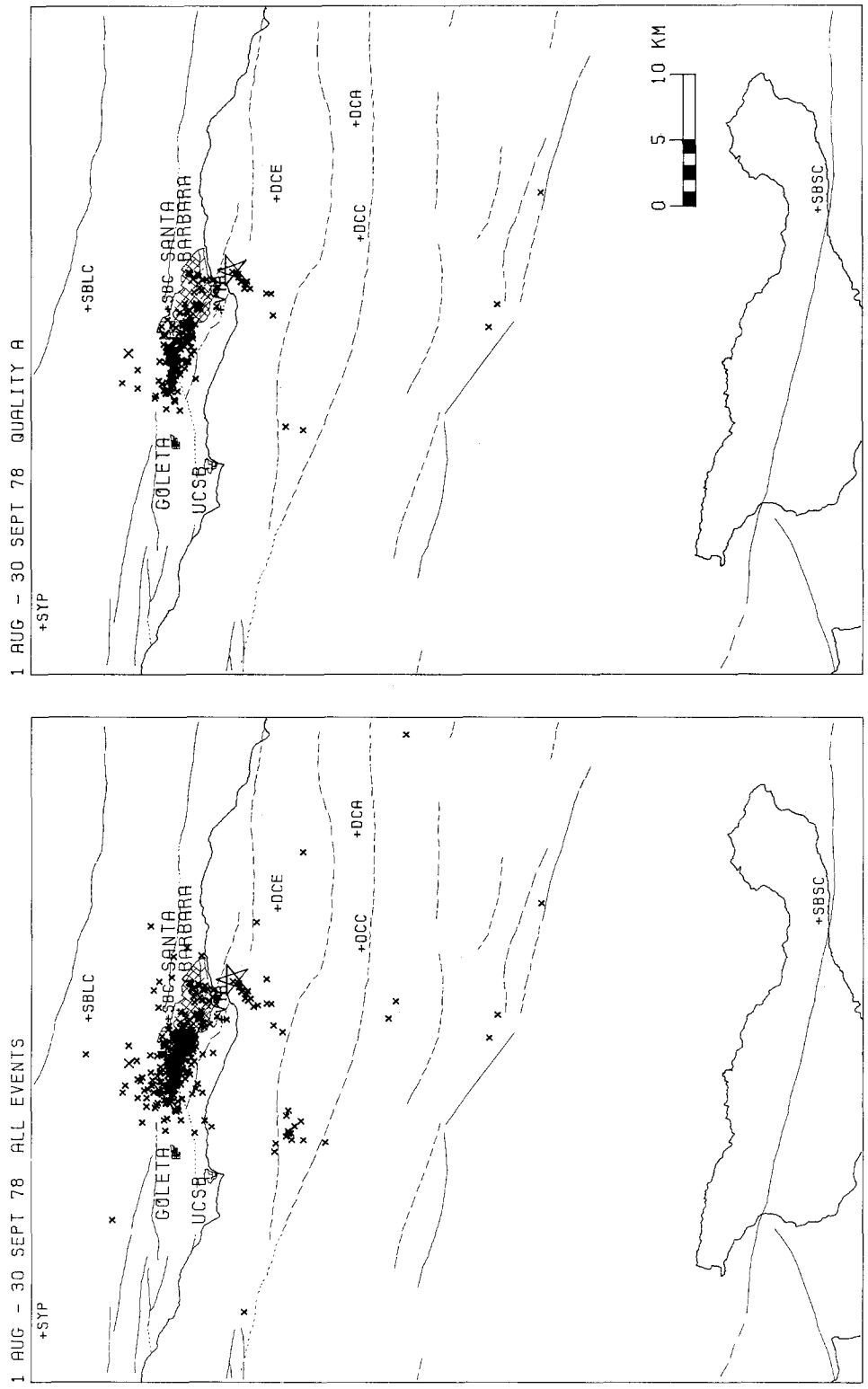

FIG. 3. Maps showing location of epicenters for August and September 1978: (*left*) all locations and (*right*) A-quality locations. Star is main shock. Small x's are events of less than magnitude 3. Large x's are of magnitude 3 to 3.5. +'s mark stations. Light, broken lines are faults after Yerkes *et al.* (1980).

higher quality data. The cluster of events located 10 km SW of the main aftershock zone is evidently due to location errors. Double checking the computer solutions for these events revealed that most of them were E-quality locations that were systematically mislocated. The two events that remain in Figure 3 (*right*) evidently are accurately located. There are also two events located SE of the main shock in Figure 3 (*left*) that suggest a lineation between the foreshock and the main shock. Checking their solutions indicates that these are also poor locations. High residuals at stations

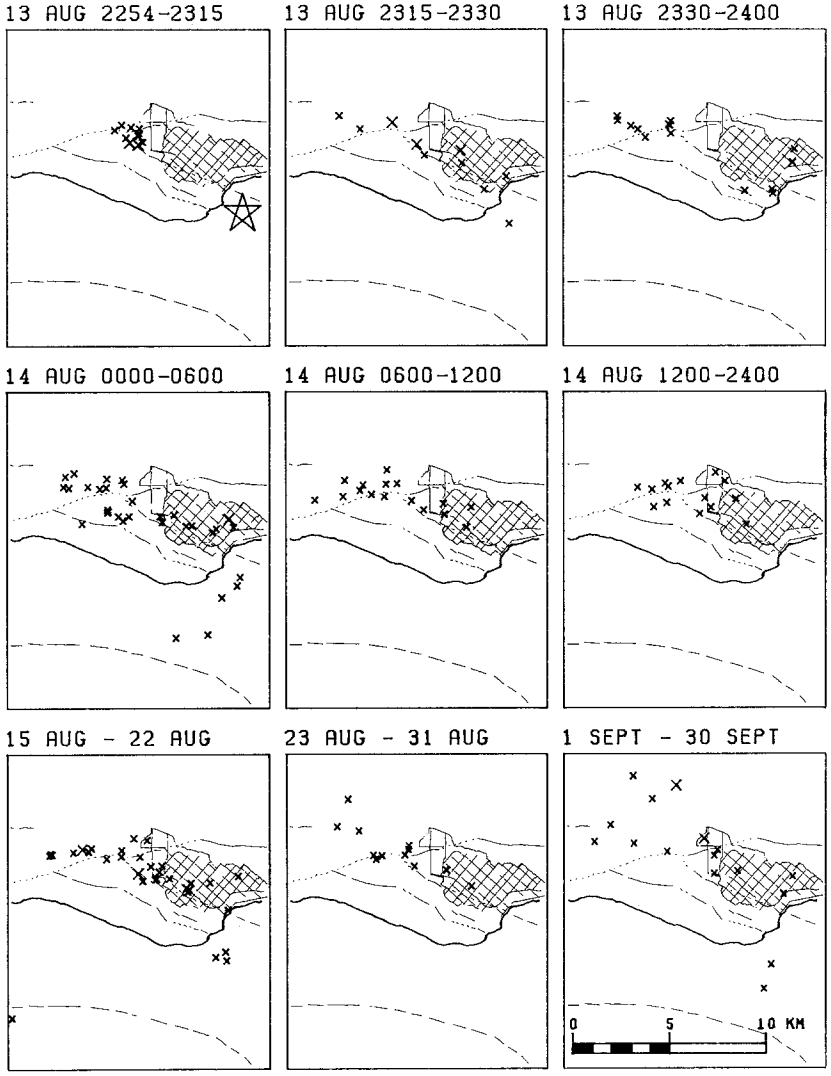

FIG. 4. Maps showing temporal development of aftershock zone. Symbols as in Figure 3.

to the east indicate that both these events are probably located within the main aftershock zone. Since there is a sufficient number of A-quality locations to delineate all the features of the aftershock zone, we will use only these highest quality locations in further discussion, so as not to muddy the waters with potentially inaccurate locations.

The aftershock location pattern had a very clear and intriguing development with time as shown in Figure 4. The most noticeable feature is that nearly all of the

aftershocks were located north and west of the main shock epicenter, and the great bulk of them were located between 4 and 10 km NW of the epicenter. All of the first recorded aftershocks, between 2300 and 2315 UTC occurred in a cluster 7 km NW of the main shock. Between 2315 and 2330 UTC, aftershocks began to fill in the zone between the main shock epicenter and the initial cluster. Between 2330 and 2400 UTC, the aftershock zone spread 3 km northward from the main shock and also extended itself another 4 km west from the initial cluster. During the following 24 hr of 14 August UTC, aftershocks further filled in the zone outlined during the first hour's activity, with a noticeable lack of activity in the spot occupied by the initial cluster. There was also relatively little activity between this point and the main shock epicenter, especially after 0600 UTC. Also, between 0000 and 0600 UTC, a new feature began to develop as aftershocks began to occur SW of the main shock epicenter. Four of these five events occurred during a 40-min period between 0046 and 0126 UTC and show a very clear migration away from the main shock epicenter toward the SW and toward the surface (Figure 5a). During the following few days, aftershock activity began to die off, but it continued to occur in the two zones outlined in the first 25 hr of activity. During the following weeks, activity died down even further, until it was averaging one detectable event per day by the end of September. A few of these latter events occurred up to 2 km farther north than the previously outlined aftershock zone. The most significant of these was a magnitude 3.4 aftershock that occurred on 12 September, 2 km north and 2 km deeper than the previous activity.

The hypocentral distribution of the aftershocks can be seen in the cross sections (Figure 5) and the stereo pair (Figure 6). These both show that most of the aftershocks outline a roughly rectangular structure that is nearly horizontal extending 11 km in the WNW direction and 4 km in the NNE direction. Contrary to normal expectations, there is less resolution of structure in the cross-dip cross section (Figure 5a) than in the cross-strike cross section (Figure 5b). This is due in part to the unusually shallow dip of the aftershock zone and in part due to the fact that the aftershock zone shallows slightly in the WNW direction, causing the apparent upward scatter in the N15°E cross section (Figure 5a). The stereo plot (Figure 6) makes this quite evident.

The cross sections also show the distribution of the aftershocks that trend SW from the main shock epicenter. They are systematically shallower to the SSW and faintly suggest a structure that dips ~55° to the NNE. This "structure" projects to the surface near the trace of the North Channel Slope-Pitas Point fault as mapped by Yerkes *et al.* (1980) (Figure 3). They indicate that this fault is a reverse fault that strikes N70°W (at this point) and dips 70°N (25 km west of this point), and has undergone movement in Quaternary time. Using these few aftershocks to tie a surface structure to activity at 13 km depth is admittedly a bit risky, but the geometry is interesting and suggestive.

Interpretation of aftershock distribution. The high resolution of the locations and timing of the main shock and aftershocks allows us to make unusually precise statements about the rupture process. The location of the main shock epicenter in the SE corner of the aftershock zone (Figure 3) strongly suggests unilateral rupture toward the NW. The clustering of all aftershocks 7 km WNW of the main shock during the first 20 min (Figure 4) then apparently marks the extent of primary rupture. The gradual increase in the aftershock zone length to 10 km during the first hour may indicate growth of the initial rupture surface through aseismic slip and aftershocks. The NE-SW extent of the initial ruptured surface is not so clearly determined, but it may be as narrow as 1 km, as indicated by the width of the initial

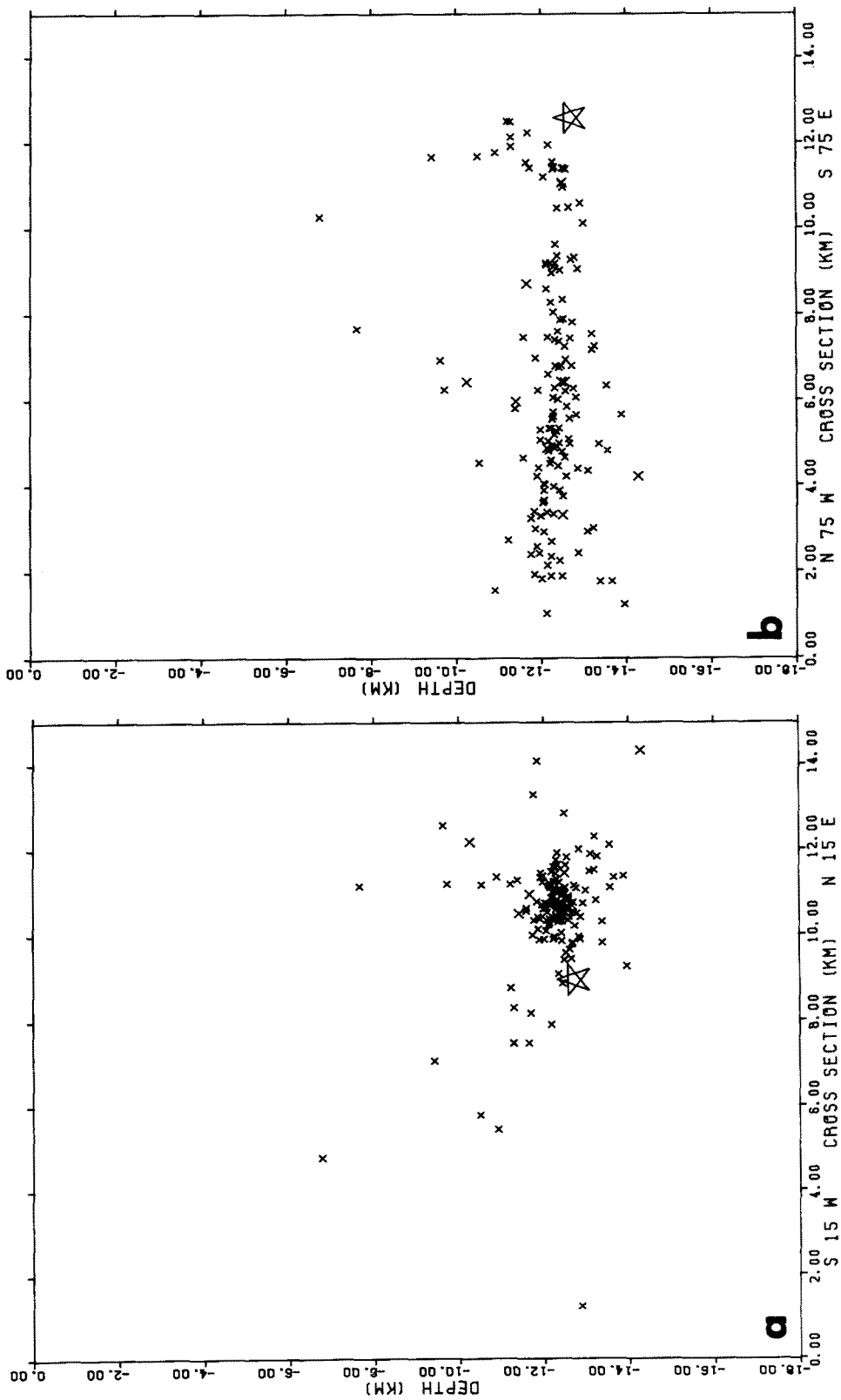

FIG. 5. (a) SSW-NNE and (b) WNW-ESE cross sections of hypocentral locations. Star is main shock. Small x's are events of less than magnitude 3, larger x's are events of magnitude 3 to 3.5.

cluster; or it may be as wide as 4 km, as indicated by the aftershock zone width after 1 hr. By the end of the first 25 hr, an area of 4 km by 11 km was clearly outlined. By the end of September, the aftershock zone had grown ~60 per cent to 6 km by 12 km (Figure 4). This observation of rupture plane growth with time illustrates the dangers of using aftershock zones to determine the size of the initial fault rupture planes.

We feel that the initial rupture may have involved as little as 7 km^2 or may have been as large as 28 km^2. An estimate based on the whole aftershock zone would have given 44 to 72 km^2 of ruptured area, which could lead to an underestimation of stress drop for the Santa Barbara earthquake. We have calculated theoretical stress drops for these fault dimensions (Figure 7), according to the formulation of Kanamori and Anderson (1975), for a circular fault (Keilis-Borok, 1959). We have used this geometry in spite of our knowledge that this was primarily a dip-slip event, because there was a significant component of strike-slip motion, and the difference in the geometric factor for different fault types is relatively small (~1.3) compared to the

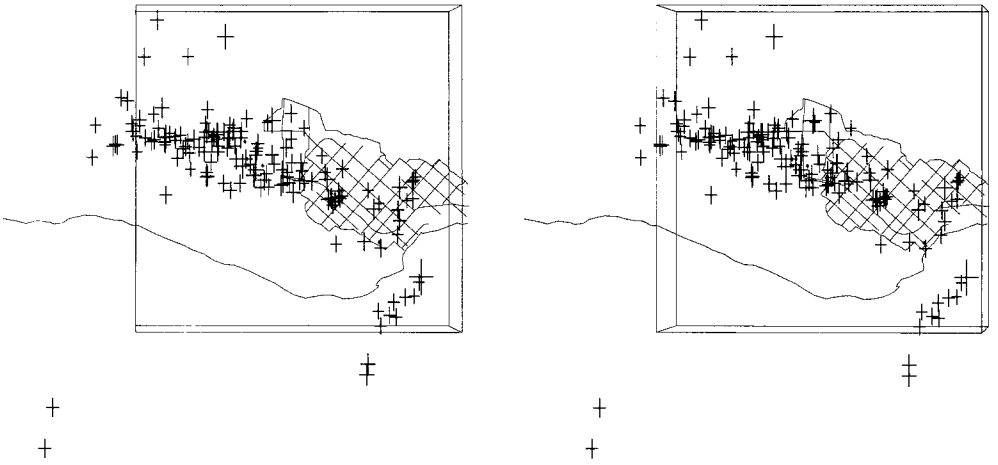

FIG. 6. Stereographic plot of main shock and aftershocks showing three-dimensional distributions of hypocenters. Crosses are scaled linearly to magnitude: main shock is the largest cross in the southeast corner. For scale, the box is 10 × 10 km and extends to 10 km depth.

other uncertainties in the problem. We have used the seismic moments of 1.1×10^{25} dyne-cm (from WWSSN short- and long-period records) and 3.6×10^{24} dyne-cm (from strong-motion records) computed by Wallace *et al.* (1981). This discrepancy in seismic moments is interesting, and may be partly explained by Ebel *et al.* (1980) who derived the time function for this event. The time function has a pair of high-amplitude spikes during the first 2 sec which are followed by a low-amplitude tail out to 6-sec duration. This may indicate that the event started as a fast (or high-stress drop) event that ruptured the first 5 to 7 km of the fault plane, but then continued as a slow (or low-stress drop) event over the remainder of the fault plane (Ebel, personal communication). Thus, the strong-motion records may represent only the high-frequency, early part of the event.

As figure 7 shows, the smaller fault area and the larger moment would give an unusually high value for stress drop (~1400 bars). We consider this only as an extreme possibility, especially since it would require an unrealistically large displacement (~5 m) for a magnitude 5 earthquake. Figure 7 was intended to show the variation in stress drop with fault area chosen (which depends on when one picks

the aftershock zone). But it also shows that the average stress drop for the whole Santa Barbara sequence decreased as a function of time. (We may neglect the seismic moment of the aftershocks since 373 magnitude 3's contribute about 1×10^{23} dyne-cm, i.e., <3 per cent of the total moment). Since we prefer the smaller fault areas for the size of the initial rupture plane, this implies that the initial rupture may have had about a meter of displacement and a stress drop of hundreds of bars. Then the fault plane may have grown by small displacement, low-stress drop activity (creep?) in the surrounding area.

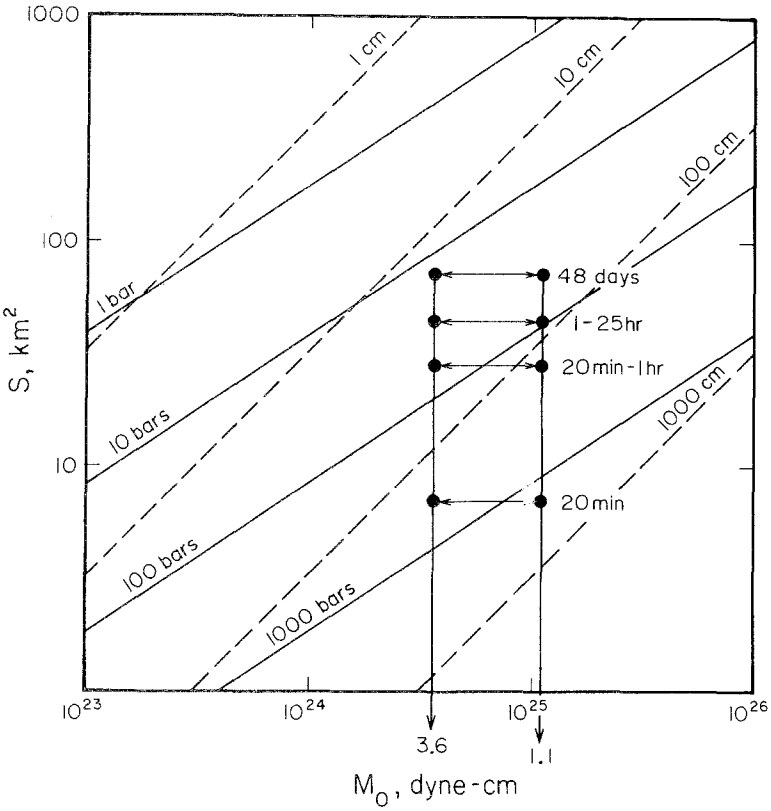

FIG. 7. Plot of seismic moment, M_0, versus area of aftershock zone, S, at different times after the main shock. Seismic moments of 3.6×10^{24} (strong motion) and 1.1×10^{25} dyne-cm (WWSSN) were calculated by Wallace *et al.* (1981). Slanted lines indicate average stress drop (solid) and average displacement (dashed) for a circular fault model.

It is interesting to note the holes in the aftershock pattern—the gaps that appear between the main shock and the main body of aftershocks. These holes appear either when we consider just the A-quality locations or all of the locations (Figure 3). It has been suggested by Wallace *et al.* (1981) that the fault breakage was rough, with several asperities. They interpret the acceleration records to indicate that the later asperities were probably located 3 and 5 km NW of the main shock epicenter, which corresponds reasonably well with the locations of areas of few aftershocks. Another asperity zone is identified by the aftershocks during the first 15 min. Apparently this was an area of stress concentration where the fault rupture either changed in character or temporarily stopped. In either case, this stuck patch had been broken through by aftershocks by 20 min after the main shock. During the 3 days following the main shock, this patch was noteworthy for its absence of

aftershocks (Figure 4). A few events occurred in this spot between 17 and 24 August, but the area became completely quiescent after that date.

The temporal development of the fault plane and the holes in the aftershock pattern suggest an aperity model for the rupture process. We feel that most of the energy released in the 5.1 M_L main shock was radiated from a few relatively small areas of the aftershock zone (probably <10 km^2) of high shear stress (possibly hundreds of bars). Then, in the ensuing hours and days, the fault extended itself into surrounding areas of low stress. The asperities having once been broken through are then areas of few aftershocks, either because of total stress relaxation or because they still have more strength than the surrounding plane. So, the aftershocks may be a better indication of where new rupture is occurring rather than where the main rupture was. This phenomenon has been observed elsewhere. Ebel (1980) suggested that the short-period energy in the Borrego Mountain earthquake of 1968 was radiated from two asperities with a few hundred bars of stress drop. And these asperity zones correspond to areas of few aftershocks.

This feature may be common to many earthquakes, but may have not been observed for a number of reasons. Perhaps when the asperities are broken, the rupture plane extends into areas of low stress very quickly, probably in a matter of minutes. Another reason is that earthquakes seldom happen where there is good station coverage. Usually, portable seismographs are not installed in the epicentral region until hours or days after activity has started. Hence, the details of locations during the first few minutes of aftershocks are usually lost. The accuracy of our locations would not have been possible except for the great good fortune of having four seismographs installed in the epicentral region the day before the earthquake.

Earthquake Magnitudes

The Caltech magnitude for the Santa Barbara earthquake was 5.1 M_L (Whitcomb and Hutton, 1978) and was based on readings from 18 Wood-Anderson-type seismographs with good agreement between readings. The University of California at Berkeley reported a magnitude of 5.7 M_L, also based on Wood-Anderson readings. Magnitudes of 5.5 m_b and 5.6 M_S were reported in the Preliminary Determination of Epicenters (PDE). The discrepancy between the Caltech M_L and the PDE readings is consistent with the observation that the WWSSN records showed a factor of 3 larger seismic moment than did the strong-motion records (Wallace *et al.*, 1981). The discrepancy in reported local magnitudes may be due in part to a directivity effect. The aftershock distribution suggests that the rupture propagated unilaterally toward the NW, which is away from most of the Caltech stations and toward the Berkeley stations. Still this is a surprisingly strong directivity effect for such a small fault, but this may argue in favor of the fault plane being quite narrow.

Magnitudes for aftershocks were calculated by Richter's method, if they were large enough to be seen on the Caltech Wood-Anderson instruments and are reported in Whitcomb *et al.* (1979). Magnitudes for the smaller aftershocks were calculated by the coda-amplitude method described by Johnson (1979). The magnitudes for the first week of activity are plotted in Figure 8. As can be seen, almost all of the energy was released in the main shock, as no aftershocks even approach it in size. Most of the aftershocks were of magnitude 3 or less, and no aftershock was larger than 3.5 M_L.

Focal Mechanisms

Focal mechanisms for the main shock, foreshock, and aftershocks were derived using P-wave first motions. Take-off angles were calculated from the same velocity

model used in the locations, and the data were analyzed with the computer program FOCPLT written by Whitcomb and Garmany (Whitcomb, 1973). This program assumes a double couple and checks all possible solutions (with a resolution of 3.5°) to minimize the number of "stations in error." The results are plotted on an equal-area projection. The program worked well for most events, but for some poorly constrained solutions, we input nodal planes that better fit the data.

Main shock. The focal mechanism for the main shock (Figure 9) is very well constrained, using first-motion data from the USC OBSs, University of California at Berkeley stations (R. Miller, personal communication) and the Caltech-USGS southern California network. The fault plane solution has one nodal plane dipping shallowly to the north (strike 280°, dip 26°, slip angle 57°), and the other dipping steeply SW (strike 135°, dip 69°, slip angle 105°), with the quadrant between them being compressional. In either case, the mechanism is indicative of compression in the NNE-SSW direction with a component of strike-slip motion. The shallow north-dipping plane is preferred as the fault plane, based on its near agreement with the aftershock distribution.

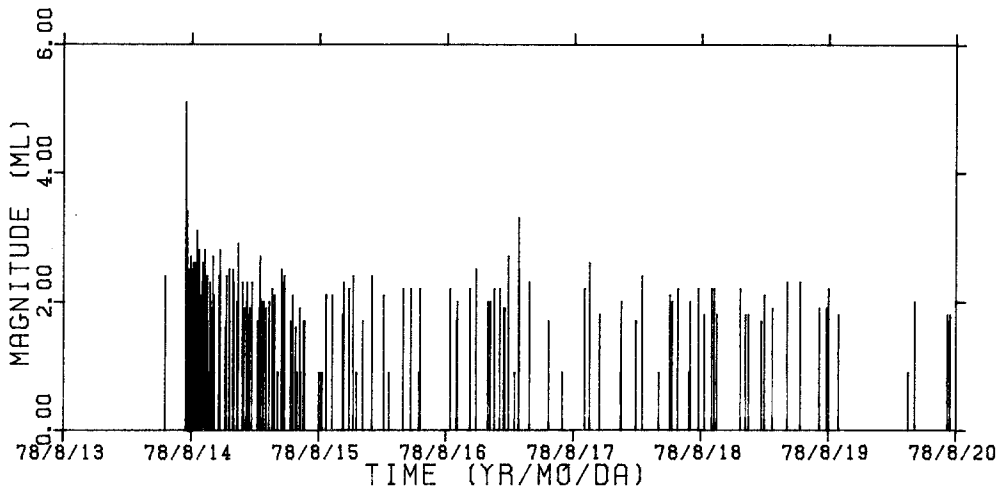

FIG. 8. Plot of magnitudes of foreshock, main shock, and aftershocks of the Santa Barbara earthquake versus time, for the first week of activity.

Because of the above-mentioned problems in modeling velocity, we have some concern that we may not have calculated take-off angles completely accurately, particularly in the N-S direction. Stations to the south, such as SBSC and SBSM, typically have large negative *P* delays, indicating that the apparent velocity in this direction is somewhat faster than our hybrid model would predict. This means that take-off angles in this direction are probably lower than the model predicts. Conversely, stations to the north, such as CRG, BCH, SBCC, and YEG have large positive *P* delays. Consequently, apparent velocities are somewhat slower, and north-going take-off angles are probably somewhat greater (i.e., more horizontal) than the model predicts. Since the shallow north-dipping plane is principally controlled by the stations CRG, SBSC, BCH, YEG, and SBCC, this nodal plane may be dipping at a shallower angle than we have calculated here.

During the process of testing velocity models for location, we also tested them to see how they influenced the main shock focal mechanism. It was noticed that models containing many layers, such as the Lee *et al.* (1978) location model (nine layers)

and Wallace's *et al.* (1981) model (10 layers) also gave a shallower dip to the nodal plane. These more smoothed velocity models may better simulate the curvature of the ray paths from the source.

Foreshock. The focal mechanism of the foreshock that occurred 4 hr before the main shock is shown in Figure 10a. As can be seen, it is nearly identical to the main shock and also indicates NNE-SSW thrusting with a component of strike-slip, in spite of being located some 23 km SE of the main shock. The mechanism is fairly well constrained and has one nodal plane dipping at 36° in the NNW direction and

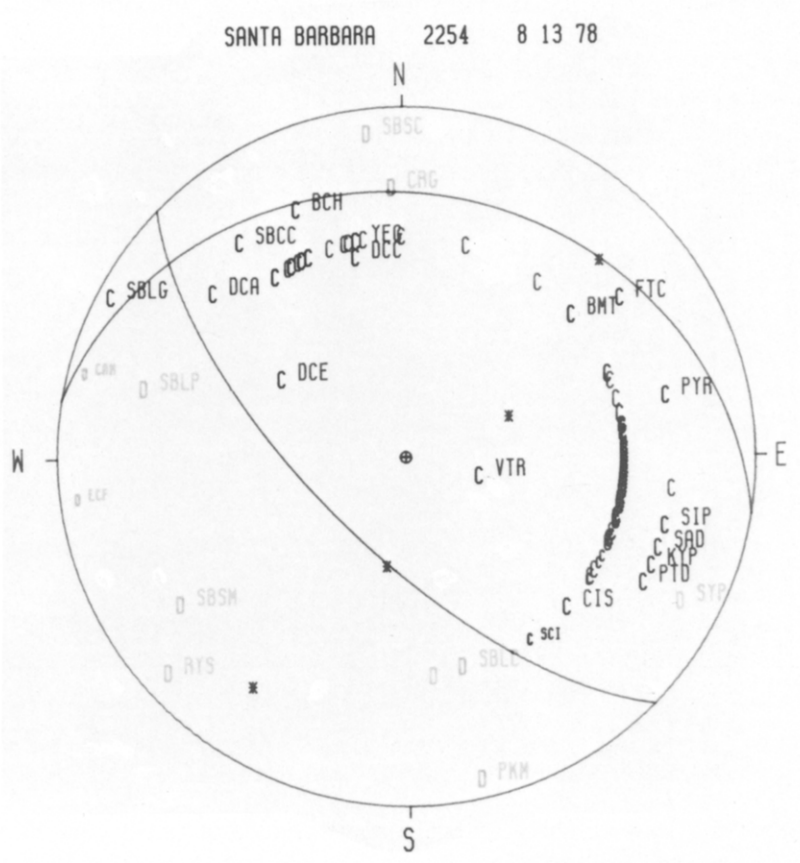

FIG. 9. Focal mechanism of the Santa Barbara main shock. Equal-area, lower hemispheric projection. C's are compressions, D's are dilatation. Three-letter designations are nearby stations.

the other dipping 61° in the SSW direction. We cannot say with confidence which plane is preferred as there is no other activity located in the area.

Aftershocks. We were able to derive reliable focal mechanisms for 46 aftershocks. We consider 24 of these solutions to be well constrained (generally more than 14 first motions and no contradictions), 20 to be fairly constrained (fewer first motions and some contradictions), and 2 to be poorly constained. These are plotted on the maps in Figure 11. Almost all of the mechanisms (40) indicate thrust movement, with the direction of thrusting varying between WNW and ENE. For most of these events, the northward-dipping nodal plane dips at 25° to 45°, in general agreement

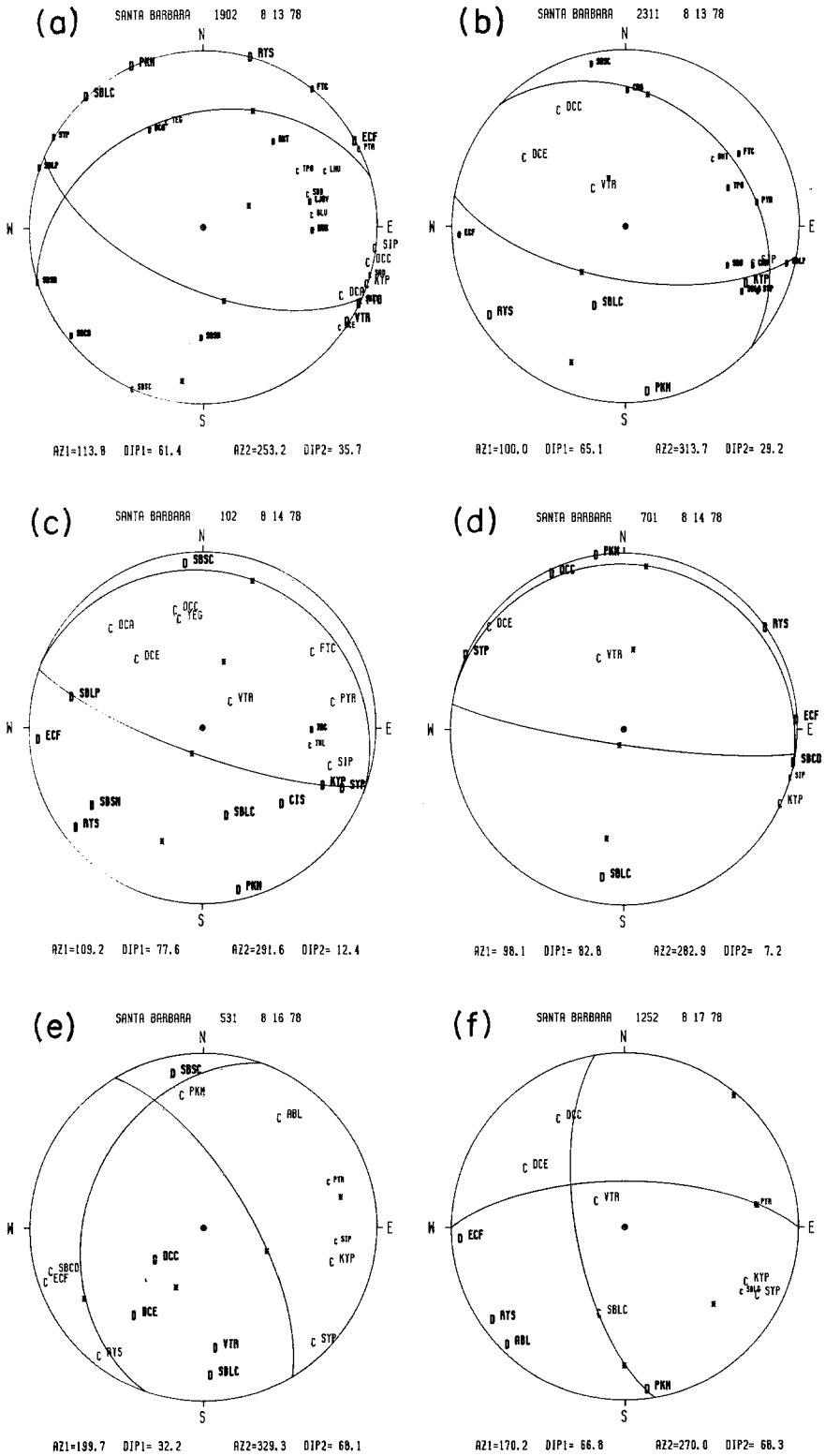

FIG. 10. Focal mechanism of foreshock and some typical aftershocks. Same projection and symbols as n Figure 9.

with the main shock focal mechanism. A typical example of one of these solutions is shown in Figure 10b.

Of particular interest are the few focal mechanisms that may indicate very low-angle thrusting. There are five in the principal aftershock zone that have a north-dipping plane with dips ranging from 7° to 15°. All five of them occur along the northern edge of the aftershock zone between the main shock epicenter and the initial aftershocks (compare Figures 4 and 11a). These are the only events we could find that exhibit a possible fault plane with a dip as low as that seen in the aftershock cross sections (Figure 5). These events occurred at 102, 633, 701, and 747 UTC on 14 August, and at 718 UTC on 18 August. Typical mechanisms of this group are shown in Figure 10, c and d. Two of these mechanisms are well constrained (102 and 701), 2 are fairly constrained (633 and 718), and 1 is fair to poorly constrained (747).

There are six focal mechanisms that are not thrust: 3 normal and 3 strike-slip (see Figure 11). Five of these six occurred relatively closely together in time, between 1655 UTC on 14 August and 1252 UTC on 17 August (i.e., on 3 days of the 48-day aftershock period we considered). This was immediately after a rather sudden decrease in the rate of aftershock occurrence (see Figure 8). So these "different" mechanisms may be related to a change in the mode of stress release at this time.

The normal mechanisms occurred first—at 1655 UTC on 14 August, and at 531 and 957 UTC on 16 August. All three mechanisms indicate E-W extension, although one (1655, 14 August) has one plane so nearly horizontal (9°WSW) that it could be considered to indicate more horizontal shearing than extension, if that nodal plane is the fault plane. One of the normal mechanisms is shown in Figure 10e.

The normal events were followed by two of the strike-slip events on 17 August, at 257 and 1252 UTC (Figure 10f). They were both located along the southern edge of the main aftershock zone (Figure 11a). The third strike-slip event occurred at 806 UTC on 5 September, 20 km south of the main aftershock zone (Figure 11b), at a depth of 19 km, making it one of the deepest events observed in this study. All three strike-slip events are compatible with horizontal compression in the NNE-SSW direction.

The significance of these "different" focal mechanisms is uncertain. During the 3-day period in which the five nonthrust events occurred, there were also three thrust events observed, as well as numerous other events that were too small to study for focal mechanisms. Three of these six "different" events are located significantly south of the main aftershock zone (Figure 11b), and hence are outside the area for which the original velocity modeling was intended. Thus, there could be some error in these fault plane solutions. Looking at the first-motion plots, however, it would take a radically different velocity model to get a thrust mechanism out of the distribution of first motions seen in plots such as Figure 10e.

Discussion

Mode of faulting. The main shock focal mechanism clearly indicates that the Santa Barbara earthquake was the result of reverse faulting. We prefer the nodal plane that dips 26° to the north as the fault plane since it most closely corresponds with the strike and dip of the aftershock hypocentral distribution. This dip, however, is somewhat greater than the dip of the aftershock zone itself (15° or less) (Figure 5a). The discrepancy may be due in part to the difficulties of velocity modeling in this area. Most of the aftershocks have north-dipping nodal planes dipping at least 25° and ranging as high as 45°, which is significantly steeper than the plane suggested by the cross sections. These planes are shown in cross section in Figure

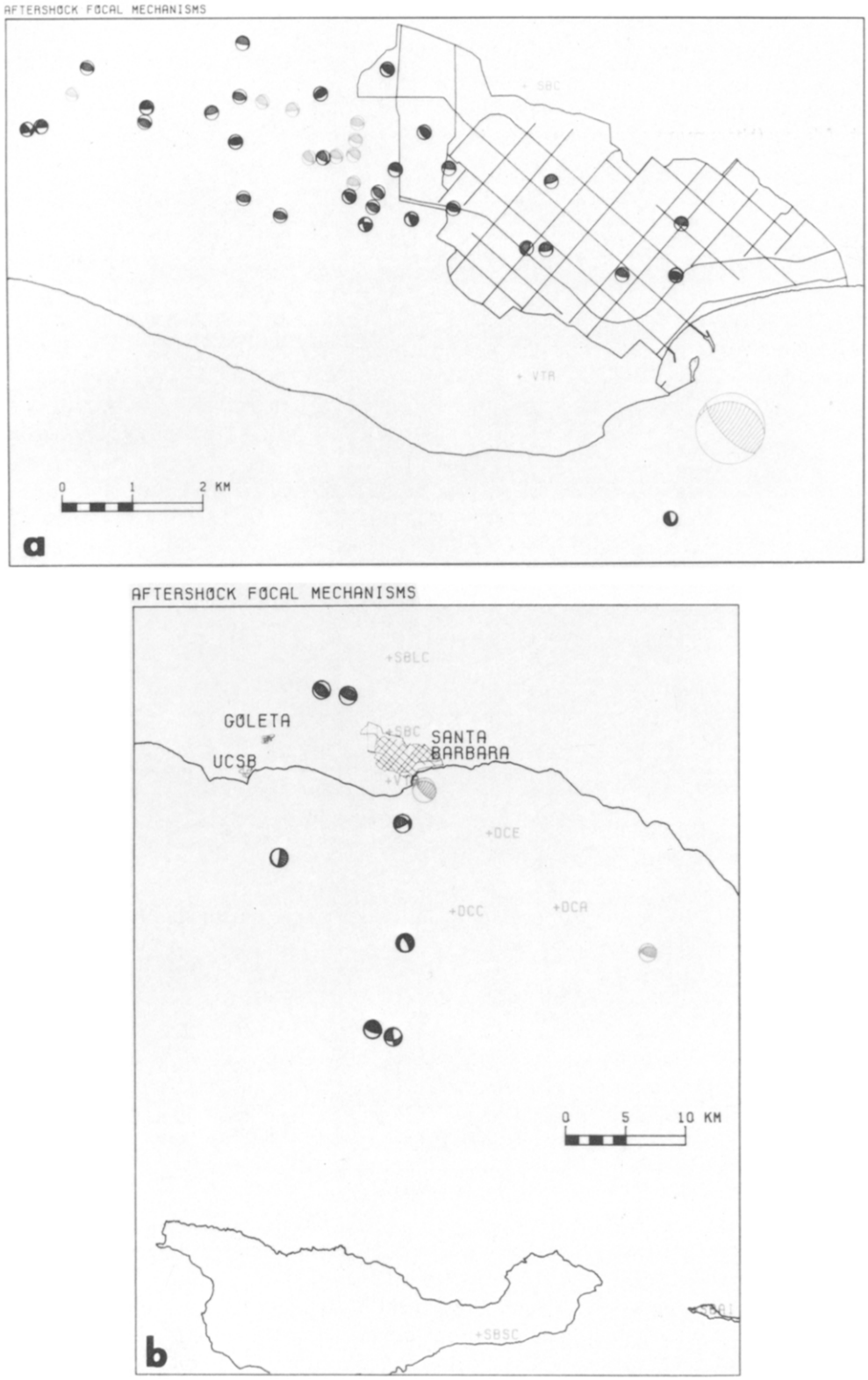

FIG. 11. Maps showing main shock and aftershock focal mechanisms located at their epicenters. (a) Large-scale map; light-colored events occurred on 13 to 14 August, dark-colored events, 15 August to 30 September. (b) Small-scale map showing main shock, foreshock, and aftershocks that would not be shown in (a).

12. Our suggestion is that this pattern indicates a complex series of imbricate thrust faults. A zone of imbricate thrusting has been previously observed nearby in a similar tectonic environment: along the south front of the Transverse Ranges near Pt. Mugu (Stierman and Ellsworth, 1976). In our case, the dip of these imbricate faults may shallow with depth into a more nearly horizontal structure. In Figure 12 there is a slight hint of such curved fault planes. This suggestion should be viewed with some caution, however, since the relative location accuracy of the events is only about 0.5 km. It seems clear, however, that the planes shown in Figure 12

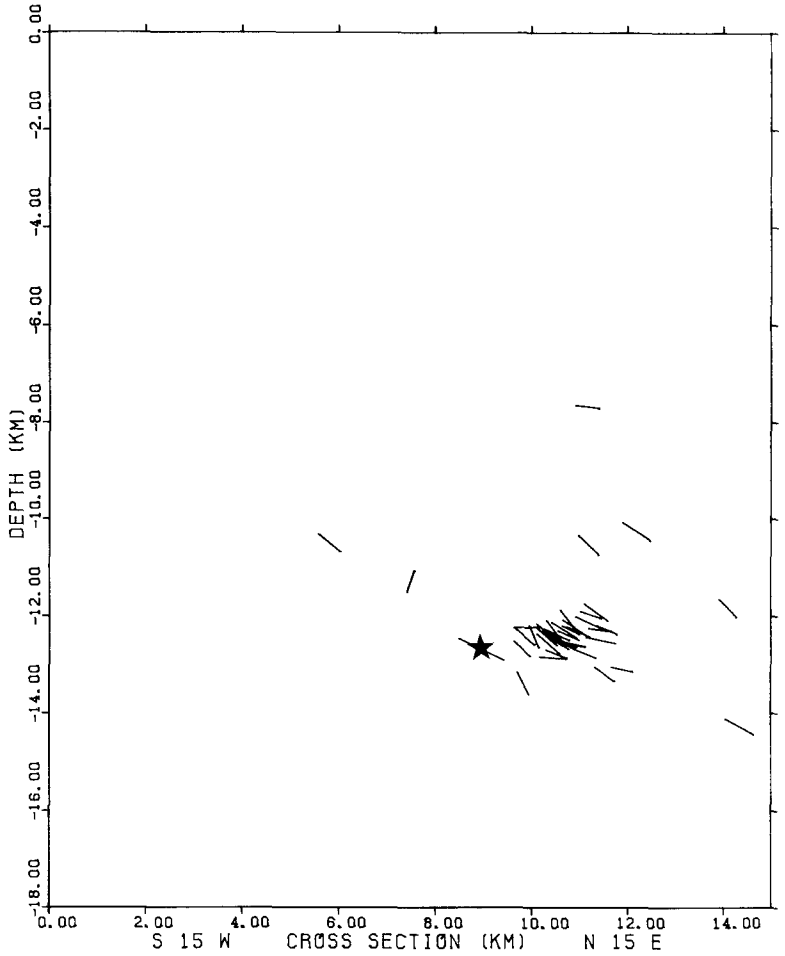

FIG. 12. SSW-NNE cross section showing orientations of preferred planes from main shock and aftershock focal mechanisms. Main shock is indicated by the star.

represent some sort of distributed shear. The N-S spread of these planes is not some artifact of choosing the wrong cross-section projection, but the result of the aftershock zone being at least 2 km wide along most of its length (see Figure 11a). The reason why these aftershock planes do not outline a single plane may be because the first-motion fault plane solutions show how the ruptures initiate but not how they progress. Thus, we are suggesting that for many of the aftershocks, the rupture initiated at the upper end of the imbricate thrust faults and propagated northward and downward. The few flat focal mechanisms that occurred along the northern

edge of the aftershock zone then might be events that initiated at the north edge of the low-angle structure and propagated southward.

Tectonic implications. One possible interpretation of our results is that the Santa Barbara area is underlain by a very low-angle thrust fault. Its complete extent is unknown, but if we project this structure upward at a dip of 15°, it would surface 48 km south of Santa Barbara, near Santa Cruz Island. This island is bisected by a known active fault; however, it is steeply dipping and its offset is evidently left-lateral rather than thrust (Weaver *et al.* 1969; Jennings, 1975; Patterson, 1978). It is unduly risky, however, to project a fault plane over such a large distance without any other supporting data. The Santa Barbara Channel is in fact cut by many steeper north-dipping reverse faults (Yerkes *et al.*, 1980) that are apparently active, and it is probably more likely that our structure curves upward into one or more of these.

Haxel and Dillon (1978) hypothesize that a large area of southern California is allocthonous and is underlain by Pelona-Orocopia schist. They suggest that the allocthon was emplaced during Paleocene or Late Cretaceous time along a single thrust fault that is extensive under the Transverse Ranges and the Mojave Desert. Several workers have expressed the idea that such a low-angle mega-thrust system may be presently active under the Transverse Ranges. Thatcher (1976) used a low-angle thrust fault to successfully model vertical displacements preceding the 1971 San Fernando earthquake. The Palmdale uplift (Castle *et al.*, 1976) may have been caused by aseismic slip of a low-angle thrust fault (Rundle, 1978; Rundle and Thatcher, 1980). Recent changes in horizontal compression across the San Andreas fault have been modeled as a horizontal southward-propagating dislocation under the Transverse Ranges, south of Palmdale (Savage *et al.*, 1981).

Hadley and Kanamori (1978) have suggested that the central Transverse Ranges are underlain by a shallowly north-dipping structure and that the San Gabriel Mountains are behaving as a decollément. They cite as evidence a pair of focal mechanisms indicating low-angle thrust at 12 km depth in the San Fernando region. Yeats (1981) has suggested that this detachment structure is extensive under the Transverse Ranges and comes to the surface in a zone of reverse faults that extends from Banning Pass to the Santa Barbara Channel region, where it appears as the Red Mountain and Pitas Point faults near Ventura. Yerkes *et al.* (1980) map the north-dipping Pitas Point fault westward across the channel to other active structures in the western Santa Barbara Channel. The Santa Barbara earthquake may have been the result of slip on such a structure, and the overlying crust here may also be a decollément.

Conclusions

We have calibrated seismographic stations in the Santa Barbara region from a seismic refraction line shot by UCSB (Crandall *et al.*, 1979) to obtain a model appropriate for earthquake locations near Santa Barbara. We have used this model to locate the 13 August 1978 Santa Barbara earthquake and all of its aftershocks to 30 September 1978. These locations suggest unilateral rupture directed toward the WNW followed by progressive growth of the fault plane with time. Hypocentral distribution and focal mechanisms for these events indicate that the earthquake was probably caused by thrust movement on a low-angle north-dipping structure 13 km under Santa Barbara. These observations suggest a tectonic model in which the western Transverse Ranges are being deformed by horizontal southward movement of the upper crust along a mid-crustal detachment surface.

ACKNOWLEDGMENTS

We thank Ken Piper, T. L. Teng, and T. L. Henyey for making the USC data available to us. We thank Barbara Bogaert and William Prothero for data regarding the UCSB seismic refraction line. We thank C. R. Allen for guidance in this study and advice on the manuscript. We are also grateful to Rob Cockerham, Tom Hearn, Dave Hill, Hiroo Kanamori, Barry Keller, Bernard Minster, Jim Pechmann, Bill Prothero, Kerry Sieh, Lee Silver, Terry Wallace, and Randy White for helpful discussion and comments on the manuscript. This work was supported by USGS Contracts 14-08-0001-19270 and 14-08-0001-16719.

REFERENCES

Bogaert, B., M. Reichle, W. Prothero, and S. Zelikovitz (1978). Aftershock study of the August 13, 1978 Santa Barbara, California earthquake, *Trans. Am. Geophys. Union* **59,** 1130.

Castle, R. O., J. P. Church, and M. R. Elliot (1976). Aseismic uplift in southern California, *Science* **192,** 251–253.

Corbett, E. J. and C. E. Johnson (1978). The Santa Barbara Channel earthquake of August 13, 1978, *Trans. Am. Geophys. Union* **59,** 1130.

Crandall, G., M. Reichle, B. P. Luyendyk, and W. A. Prothero (1979). Marine seismic refraction study of the Santa Barbara Channel (Southern California Borderlands), *Trans. Am. Geophys. Union* **60,** 886.

Ebel, J. E. (1980). Evidence for fault asperities from systematic time-domain modeling of teleseismic waveforms, *Ph.D. Thesis,* California Institute of Technology, Pasadena, California, 141 pp.

Ebel, J. E., D. V. Helmberger, and T. C. Wallace (1980). Evidence for fault asperities from the analysis of near-field and teleseismic waveforms, *Trans. Am. Geophys. Union* **61,** 1027.

Gardner, J. K. (1962). Earthquakes in the Walker Pass region, California, and their relation to the tectonics of the southern Sierra Nevada, *Ph.D. Thesis,* California Institute of Technology, Pasadena, California, 122 pp.

Hadley, D. and H. Kanamori (1978). Recent seismicity in the San Fernando region and tectonics in the west-central Transverse Ranges, California, *Bull. Seism. Soc. Am.* **68,** 1449–1457.

Hamilton, R. M., R. F. Yerkes, R. D. Brown, Jr., R. O. Burford, and J. M. DeNoyer (1969). Seismicity and associated effects, Santa Barbara region, *U. S. Geol. Surv. Profess. Paper 679,* 47–68.

Haxel, G. and J. Dillon (1978). The Pelona-Orocopia schist and Vincent-Chocolate Mountain thrust system, southern California, in *Mesozoic Paleogeography of the Western United States,* D. G. Howell and K. A. McDougall, Editors, Soc. Econ. Paleo. Min. Pacific Section, 453–469.

Healy, J. H. (1963). Crustal structure along the coast of California from seismic-refraction measurements, *J. Geophys. Res.* **68,** 5777–5787.

Henyey, T. L., J. K. McRaney, D. V. Manov, and T. L. Teng (1978). The 1978 Santa Barbara earthquake as recorded by an offshore seismic network, *Trans. Am. Geophys. Union* **59,** 1130.

Jennings, C. W. (1975). Fault map of California, *Calif. Div. Mines and Geology, Geology Data Map 1* scale 1:750,000.

Johnson, C. E. (1979). CEDAR—An approach to the computer automation of short-period local seismic networks, *Ph.D. Thesis,* California Institute of Technology, Pasadena, California, 332 pp.

Johnson, C. E. and D. M. Hadley (1976). Tectonic implications of the Brawley earthquake swarm, Imperial Valley, California, January 1975, *Bull. Seism. Soc. Am.* **66,** 1133–1144.

Kanamori, H. and D. L. Anderson (1975). Theoretical basis for some empirical relations in seismology, *Bull. Seism. Soc. Am.* **65,** 1073–1095.

Keilis-Borok, V. I. (1959). On estimation of the displacement in an earthquake source and of source dimensions, *Ann. Geofis.* **12,** 205–214.

Lee, W. H. K. and J. G. Vedder (1973). Recent earthquake activity in the Santa Barbara Channel region, *Bull. Seism. Soc. Am.* **63,** 1757–1773.

Lee, W. H. K., C. E. Johnson, T. L. Henyey, and R. F. Yerkes (1978). A preliminary study of the Santa Barbara, California earthquake of August 13, 1978 and its major aftershocks, *U. S. Geol. Surv. Circular 797,* 11 pp.

Lee, W. H. K., R. F. Yerkes, and M. Simirenko (1979). Recent earthquake activity and focal mechanisms in the western Transverse Ranges, California, *U. S. Geol. Surv. Circular 799,* 1–26.

Patterson, R. H. (1978). Neotectonics of the Santa Cruz Island fault, California, *Earthquake Notes* **49,** 21.

Rundle, J. B. (1978). Gravity changes and the Palmdale uplift, *Geophys. Res. Letters* **5,** 41–44.

Rundle, J. B. and W. Thatcher (1980). Speculations on the nature of the southern California uplift, *Bull. Seism. Soc. Am.* **70,** 1869–1886.

Savage, J. C., W. H. Prescott, M. Lisowski, and N. E. King (1981). Rapid aseismic strain change observed on the San Andreas fault near Palmdale, California, *Science* **211,** 56–58.

Stierman, D. J. and W. Ellsworth (1976). Aftershocks of the February 21, 1973, Pt. Mugu, California earthquake *Bull. Seism. Soc. Am.* **66,** 1931–1952.

Sylvester, A. G., S. W. Smith, and C. H. Scholz (1970). Earthquake swarm in the Santa Barbara Channel, California, 1968, *Bull. Seism. Soc. Am.* **60,** 1047–1060.

Thatcher, W. (1976). Episodic strain accumulation in southern California, *Science* **194,** 691–695.

Vedder, J. G., H. C. Wagner, and J. E. Schoellhamer (1969). Geological framework of the Santa Barbara Channel region, *U. S. Geol. Surv. Profess. Paper 679,* 1–12.

Wallace, T. C., D. V. Helmberger, and J. E. Ebel (1981). A broad-band study of the August 13, 1978 Santa Barbara earthquake, *Bull. Seism. Soc. Am.* **71,** 1701–1718.

Weaver, D. W., D. P. Doerner, and B. Nolf (1969). Geology of the Northern Channel Islands, Special Pub: Am. Assoc. Petrol. Geol. and Soc. Econ. Paleo. Min. Pacific sections, 200 pp.

Whitcomb, J. H. (1973). The 1971 San Fernando earthquake series, focal mechanisms and tectonics, *Ph.D. Thesis,* California Institute of Technology, Pasadena, California, 443 pp.

Whitcomb, J. H. and L. K. Hutton (1978). On the magnitude of the August 13, 1978, Santa Barbara, California earthquake, *Trans. Am. Geophys. Union* **59,** 1130.

Whitcomb, J. H., C. R. Allen, *et al.* (1979). Caltech-USGS monthly preliminary epicenters from March 1978 to January 1979, Seismological Laboratory Report, California Institute of Technology, Pasadena, California.

Yeats, R. S. (1981). Quaternary flake tectonics of the California Transverse Ranges, *Geology* **9,** 16–20.

Yerkes, R. F. and W. H. K. Lee (1979). Late Quaternary deformation in the western Transverse Ranges, California. *U. S. Geol. Surv. Circular 799,* 27–37.

Yerkes, R. F., H. G. Greene, J. C. Tinsley, and K. R. Lajoie (1980). Seismotectonic setting of the Santa Barbara Channel area, southern California, *U. S. Geol. Surv., Open-File Rept. 80–299,* 24 pp.

SEISMOLOGICAL LABORATORY
CALIFORNIA INSTITUTE OF TECHNOLOGY
PASADENA, CALIFORNIA 91125
CONTRIBUTION NO. 3589 (E.J.C.)

U.S. GEOLOGICAL SURVEY
SEISMOLOGICAL LABORATORY
CALIFORNIA INSTITUTE OF TECHNOLOGY
PASADENA, CALIFORNIA 91125 (C.E.J.)

Manuscript received 14 July 1982